Dynamic Balancing of Underactuated Robots

by

Ayşe Neşe Tüfekçiler

Submitted to the Graduate School of Engineering and Natural Sciences
in partial fulfillment of
the requirements for the degree of
Master of Science

Sabancı University

Fall 2009

Dynamic Balancing of Underactuated Robots

APPROVED BY

Assist. Prof. Dr. Volkan Patoğlu .....
(Thesis Supervisor)

Assist. Prof. Dr. Ahmet Onat .....
(Thesis Co-Supervisor)

Assist. Prof. Dr. Kemalettin Erbatur .....

Assist. Prof. Dr. Esra Erdem .....

Assist. Prof. Dr. Ali Koşar .....

Assist. Prof. Dr. Kürşat Şendur .....

DATE OF APPROVAL: .....

to my family

Acknowledgments

First and foremost, I would like to thank my supervisor Volkan Patoglu, for his tireless support and encouragements throughout my study. I am truly grateful for his patience and kindness.

Secondly, I wish to express my sincere thanks to my co-advisor Ahmet Onat for his involvement in my studies. I am grateful for his comments, suggestions and advice with his total patience and kindness.

I would like to thank my lab mates for their total support. I especially thank to Ender Kazan and Cagrı Gürbüz. I am thankful to the Human-Machine Interaction lab mates for their total support and educational contributions.

At most, I would like to express my thanks to my family for their encouragement and support throughout my life. Their belief in me have always encouraged me. They fostered my interests and my educational studies throughout my life.

Last but not least, my special thanks are due to Erdem Öztürk for his supportive attitude and kindness. I am grateful to him for enriching my life.

Abstract

This thesis presents the control of planar underactuated systems that have one less control input than the number of degrees of freedom. The underactuated robots are studied to achieve dynamically stable motions commonly encountered during robot locomotion. This work emphasizes the relation between the underactuated systems and biped locomotion and builds on the previous works in the literature on underactuated robot locomotion.

Two planar system models are treated: an acrobatic robot and a compass biped with torso. The dynamic stability of fast periodic trajectories of these systems are regulated by designing asymptotically stable feedback controllers. The resulting internal dynamics of the systems are analyzed and shaped to achieve energy efficiency and robustness of the closed-loop system trajectories. In particular, Bézier polynomial approximations and parameter optimization methods are used to systematically construct the internal dynamics of the systems. Simulation results are presented for dynamically stable orbits of the acrobatic robot and the compass biped with torso.

Özet

Tahrik derecesi serbestlik derecesinden az olan düzlemsel mekanik sistemlerin kontrolü zor bir problemdir. Bu mekanik sistemler iki ayaklı robotlarda sıkça rastlanan dinamik kararlı hareketi modellemek için kullanılmaktadır. Bu çalışmada serbestlik derecesinden sayıca az tahrikli sistemler ile iki ayaklı yürüyen robotlar arasındaki bağlantı ele alınmıştır.

İki adet düzlemsel sistem modeli incelenmektedir; bunlar akrobatik robot ve yürüyen robottur. Bu sistemlerin hızlı periyodik yörüngelerinin dinamik kararlılıkları asimtotik kararlı geribesleme kontrölörleriyle gerçekleştirilmiştir. Oluşan sistemin iç dinamikleri incelenip enerji tasarrufu ve kapalı-çevrim gürbüz kontrol sağlamak için şekillendirilmiştir. Özellikle, sistemin iç dinamiğini şekillendirmek için sistematik olarak Bézier polinom yaklaşımları ve parametre optimizasyon yöntemleri kullanılmıştır. Simulasyon sonuçları, akrobatik robot ve yürüyen robotun dinamik kararlı yörüngelerini sunmaktadır .

Table of Contents

List of Figures

List of Tables

Chapter 1

Introduction

This thesis covers the design of nonlinear controllers for a class of underactuated mechanical systems to simulate dynamic balancing and biped locomotion. The mathematical models of these systems, their corresponding feedback controllers and stability analysis are presented. The robot models studied in this work are simple, yet they capture the important aspects of dynamic balancing and biped locomotion.

1.1 Motivation

Locomotive robots with the purpose of operating in unstructured environments motivated studying biped robots. In the design of these robots, the central issue is stability where static equilibrium is not achieved at each instant of time due to gravity and the free moving feet. Dynamic stability problems are inherent to these type of systems such that they have unpowered interaction with the world. In order to get an accurate understanding of dynamic stability with no statically stable motions, it is instructive to explore the behavior of underactuated mechanical systems. The existence of uncontrollable degrees of freedom in underactuated mechanical systems is a characteristic complexity in the case of stability. Considering these, an overview in literature on control of simple underactuated systems, biped robots and their control methodologies are given.

1.2 Underactuated Systems

Underactuated systems possess less degrees of actuation than their independent configuration variables. These systems may exhibit complex internal dynamics and lack feedback linearizability; therefore, their control has been a challenging subject

in robotics.

Inverted-pendulum type underactuated systems have been used as the most common testbeds to study underactuated control architectures. The problems studied include swing-up of the pendulum from its downward position to upward equilibrium and then switching to a linear controller for balancing around this equilibrium [57]. A similar example uses energy based methods for swing-up control [52] of the Acrobot [51], a robot represents the example of a gymnast on a high bar. Other studies on underactuated systems using energy based methods include balancing of the Pendubot [55], the cart-pole system [10], and the rotating inverted pendulum [1]. Hauser and Murray further studied the Acrobot in [24] where they applied approximate linearization to move the Acrobot through the set of inverted equilibrium positions. Another related approach proposed in [5] is the design of balancing controller with the use of spline approximations. Some other Acrobot related works are considered in [2], [52]. These approaches include partial feedback linearization as an initial step for control of underactuated systems.

The studies on underactuated mechanical systems also include the control of the brachiating robots that are proposed in [34], [48]. Saito *et al.* used feedforward methods to control a two-link robot brachiating on a ladder while in [34] the dynamic task is encoded by a lower dimensional system with feedback methods.

Passivity-based methods are other popular approaches that are applied to the swing-up control problem of underactuated systems, such as inverted pendulums [52]. The drawback of this approach can be named as the lack of experimental applications. Some other methods are adaptive control [22] and sliding mode control techniques [58] which have been also applied to underactuated systems with limited applications.

Underactuated mechanisms are interpreted by some researchers as systems with second order nonholonomic constraints. The stability of these systems are achieved with continuously differentiable state feedbacks [6] and [47].

In addition to the traditional methods, hybrid and switching-based control methods have been adopted recently in control of underactuated mechanical systems and bipedal locomotion of walking robots [53],[54].

1.3 Biped Locomotion

There have been numerous studies in literature over legged locomotion. Legged robots range from multi-legged robots to one-legged hoppers. In the design of these systems, stability is the main concern. For example, if the robot loses its stability, it can fall and damage its environment. So understanding and control of stability has crucial importance. The notion of stability can be classified into three categories: static stability, quasi-static stability and dynamic stability. In static stability, the objective is to keep the center of mass within the support area of its contact on the ground. Robots with multi-legs can achieve static stability while lifting one or more legs and still keep their static balance. In quasi-static stability, robots can demonstrate static stability with limited dynamic behavior and their center of pressure usually needs to stay in their support area. In dynamic stability, the robot's center of mass leaves the support area of its contact during its motion.

Since the objective of this study is to achieve dynamically balanced walking in legged locomotion, further discussion covers analysis and literature overview on biped robots.

A biped robot is an open kinematic chain which can have one or two contacts with the ground. The robot consists of links which represent the legs and torso connected at a joint called the hip. The leg that is contacting with the ground is named as the stance leg and the other link is called the swing leg. The foot of the robot can be classified as a point or a flat foot.

Bipeds generally have high degrees of freedom and they tend to have big flat feet and full actuation. These robots demonstrate static or quasi-static walking. But, with the design of unactuated ankles meaning point footed designs, true dynamic motions can be studied.

In literature, bipeds are generally categorized according to their types of actuation such as unactuated and actuated bipeds. Unactuated bipeds are the passive ones where the gravity powers walking whereas actuated bipeds require external power source.

McGeer researched on passive walking [37] and he showed that bipeds could move dynamically without the need of actuation, only using the potential energy that was gained while walking down a slope. Some examples of passive-dynamic machines are

included in references [19], [16], [17], [11]. In passive walking, the energy loss with the heel-strike collision is compensated by the work done by the gravity. The lost energy of passive-dynamic machines can also be provided with minimum actuation where actuators does enough to provide the lost energy. For example, stable and periodic dynamic walking on level ground can be achieved with minimum actuation as proposed in [43], [12], [56].

Besides passive walking, recently there is considerable effort in the development of actuated biped robots. With actuated bipeds relatively more versatile and human like machines are intended to develop. Some of the research on fully actuated bipeds can be named as Waseda University robot [31], MIT Leg Lab robot named Spring Flamingo [42], the Technical University of Munich biped Johnie [18], the BIP at INRIA [14] and Sabancı University biped SURALP [13]. These robots are shown to achieve effective and robust locomotion. However, the fully actuated bipeds tend to rely on a characteristic bent knee stance support with a flat foot restriction, making the walking control different than the one generally employed by humans.

For obtaining an efficient and more natural looking bipedal gait, in literature researchers have investigated dynamic walking. In dynamic bipedal walking, the ground contacts are considered inherently unilateral and underactuated. To address this behavior, underactuated robots are studied in legged locomotion. In literature, some of the research on underactuated bipeds are [15], [8], [40], [36], [7].

The mostly adopted control strategy in the actuated bipeds is based on the zero moment point (ZMP) principle [60] where ZMP is kept within the safe area of the support polygon. With ZMP, the dynamic motions such as dynamic walking or running can not be achieved. For example Honda's sophisticated humanoid robot [25] demonstrates of this approach, however the quasi-static walking is not human like and is inefficient. Actuated dynamic walking approaches that do not use the ZMP principle are also proposed in literature. Pratt *et al.* introduced a virtual model control strategy where the aim is to exploit the natural dynamics of the biped [42]. One other approach is on the concept of hybrid zero dynamics [61].

In the literature, control algorithms of most of these robots are through trajectory tracking, where the trajectories are generated off-line or on-line with a high level motion planner. The most commonly used control algorithms have time-dependent

trajectories and make use of PID control [39], computed torque method and sliding mode control [38], [41], [46] to track the trajectories.

In addition to tracking time-dependent trajectories, bipeds can also be controlled with time-independent tracking algorithms. In [40], dynamic walking is achieved with a single actuator and the trajectory is slaved to the robot's state. In [21], the walking is controlled by imposing constraints on the biped which are parameterized by the robot's state. The RABBIT is controlled through trajectory tracking by time-scaling the pre-computed trajectories [7]. Some other control methods include controlling energy and the angular momentum [26], [27], [19], [33], [44], [45], [49].

A classical technique to analyze the dynamics of these robots is done through Poincaré maps. Poincaré sections are used to study the stability of walking. This approach has been applied in literature to passive walkers [19] and bipeds [26], [27].

1.4 Objectives and Organization

This section presents the main objectives and organization of this thesis.

The main focus of this thesis is on applications of feedback control for stable periodic motions in the class of underactuated systems. Raibert's biomechanically inspired design [45] has the initial influence on this thesis since his dynamically balancing one-leg hopper had been very successful and become pioneering in the locomotion literature where the design of dynamically balancing walkers are still considered an open problem.

To achieve a human like walking in robot locomotion, dynamic aspects of locomotion need to be considered. This challenge comes with the nature of the foot contact with the ground. In traditional robot walking, biped has flat foot which restricts tipping over and constraints the biped to move statically or quasi-statically as in ZMP method. ZMP method enforces the flat foot to stay on the ground without tipping over. On the other hand, in natural human walking, the foot can tip over on one of its edges and it can only exert compressive forces to the ground and thus this makes the system underactuated. Therefore, the underactuated mechanical systems will be investigated to achieve dynamic balancing tasks in biped locomotion.

In this thesis, two simple planar underactuated systems are presented for studying the dynamic aspects of biped locomotion. The dynamically stable motions

include the balancing and walking tasks. A two-link robot, that consists of two revolute rigid links without actuation between the ground and the robot, is treated for studying the balancing task in biped locomotion. The balancing task includes stabilizing the system at its static equilibrium condition where the system is at rest at its intended position such that sum of all forces and torques applied to it is equal to zero. And one other balancing task is to stabilize the system around its equilibrium such that the system tracks periodic stable orbits achieving dynamic motions where the center of mass of the robot lies outside the support base during its motion. Next, a three-link robot is presented for studying the walking task. The three-link robot consists of three revolute rigid links without any actuation at the joint connecting the robot to the ground. The walking task is different than the balancing task which has the condition of support change with impacts. During walking, the dynamically stable motions are desired since the system has point contact condition with the ground and underactuation.

The control approach for the balancing and walking tasks includes trajectory tracking by developing feedback controllers. For the first balancing task, the system is enforced to converge to the desired trajectory using partial feedback linearization and then a linear controller is applied to stabilize it around its equilibrium. For the second balancing task and the walking task, output functions are defined and setting these to zero constraints the systems to move in the desired trajectories. The outputs are first expressed in an intuitive manner and then are parameterized using polynomials. The parametrization of the trajectories with polynomials enables the trajectories to be systematically designed using parameter optimization techniques. Finally, the behaviors of the systems are studied through their stability analysis.

The thesis is organized as follows:

In Chapter 2, the dynamic models treated by this thesis are presented. Several approaches covering set-point and trajectory tracking control of underactuated systems are covered throughout Chapters 3-5. In particular, Chapter 3 introduces an example of an underactuated mechanical system named Acrobot which will be used to present the key points developed in the later chapters. Set-point control method is applied to stabilize the Acrobot around its unstable equilibrium point by using a linearization-based technique. Chapter 4 uses the results of Chapter 3 to tackle the

problem of underactuation in control. A trajectory tracking controller is provided in order to track time-invariant periodic orbits on the Acrobot example. The control design procedure covers achieving a continuous trajectory by using partial feedback linearization method that is applied on the model to drive a set of outputs to zero and analyzing the system's resulting dynamics. The outputs are shaped to result in the desired internal dynamics. In Chapter 5, a three-link robot is presented to study the walking task. In this case, the time-invariant trajectory is completed with an impact map to form a walking motion. The control inputs are used here to set the outputs to zero. The outputs are designed together with the impact map to reach a periodic stable orbit. Additional to an intuitive approach for output design, a dynamic optimization approach is used to parameterize the outputs. The stability of the trajectory is studied by using Poincaré mapping. Chapter 6 concludes the thesis and discusses future work. The derivations of the equations of motion of Acrobot are given in Appendix A. Finally, Appendix B presents the equations for conservation of angular momentum at impact.

Chapter 2

Modeling

In this chapter, the modeling of the underactuated robots that are utilized in this work are introduced. These underactuated systems possess one less degree of actuation, with no actuation at the point connecting the stance leg to the ground. Such robots consist of open kinematic chains and have motion only in the sagittal plane.

The dynamics of motion is partitioned into two phases, swing phase and impact phase. Swing phase describes the dynamics during single point contact with the ground, while impact phase describes the collision of the kinematic chain with the impact surface. To reach a walking model, the swing phase model is derived and combined with the impact model to achieve the dynamic model of the successive phases of motion. In the case of switching between these phases, the transition from one phase to the next is assumed to take place in an infinitesimal amount of time [50].

The outline of this chapter is as follows. First, the swing phase model is presented with the standard models for underactuated systems in Section 2.1. Then, the impact model is explained in Section 2.2. In Section 2.3, the complete equations of motion of the system with impacts are derived. Sections 2.4 and 2.5 cover two examples of underactuated systems.

2.1 Swing phase model

The swing phase model consists of an open kinematic chain with single point contact with the ground. The equations of motion are derived by applying the Kane's method. The state space of the model is n dimensional and the state vector

is $q = (q_1, \ldots, q_n)$. The equations of motion for an underactuated mechanical system are as follows

$$M(q)\ddot{q} + C(q, \dot{q})\dot{q} + G(q) = Bu, \tag{2.1}$$

where M is the mass matrix, C is the Coriolis matrix, G is the gravity matrix, B is the linear mapping from torques to configurations and u is the control input. The second order system is written in state space form as

$$\dot{x} = \begin{bmatrix} \dot{q} \\ M^{-1}(q)[-C(q, \dot{q})\dot{q} - G(q) + Bu] \end{bmatrix} \tag{2.2}$$

where $x = (q', \dot{q}')'$.

2.2 Impact model

The impact occurs when the swing leg touches the ground. After the collision with the ground, the legs swap their coordinates and velocities under the rigid contact model. The old stance leg becomes the new swing leg, while the old swing leg becomes the new stance leg. In Appendix B, the conservation of angular momentum equations are derived. The result of the impact is

$$x^+ = \Delta x^-, \tag{2.3}$$

where x^+ and x^- represent the state values just after and just before impact and the Δ is the function that describes the impact event.

2.3 Switching model

The swing phase model is combined with the impact model to introduce a non-linear system with impulse effects [28], [21]

$$\dot{x} = f(x) + g(x)u \qquad x^- \notin S \tag{2.4}$$

$$x^+ = \Delta x^- \qquad x^- \in S \tag{2.5}$$

where the switching condition is set as

$$S = \{(q, \dot{q}) \in X \mid h = 0, L > 0\}. \tag{2.6}$$

The swing phase model undergoes impact when the states reach the set S. X corresponds to the physically reasonable configurations of the robot. At the switching surface, the value of h, defining the swing leg end-point height from ground, is equal to zero and the value of L, corresponding to the swing leg end-point distance from the contact-point, needs to be positive. The symbol t_e defines the time of the impact. The solution of the hybrid model exists if there is a finite time $t_e > 0$ where $\delta \in X$ is the solution of the swing phase dynamics.

To produce one complete motion, the robot starts from an impact phase (double support) and ends in an impact phase. The legs swap their configurations and only one impact with the ground occurs through this cycle with the non-physical assumption that the swing foot can pass through ground when the stance leg is near vertical.

2.4 Case Study 1: The two-link planar robot, Acrobot

The model used here is a representative of the Acrobot [5], [51]. A rigid two-link planar robot with revolute joints and a single actuator at the hip is shown in Figure 2.1. The connections between the links are assumed to be implemented using frictionless hinges. The motion of the model is governed by the classical laws of rigid body dynamics. The parameter values used in simulations are given in Table 2.1.

Parameter	Label	Value	Unit
point mass	M_1	7	kg
point mass	M_2	7	kg
leg length	l_1	0.5	m
leg length	l_2	0.75	m
center of mass length	l_{c1}	0.5	m
center of mass length	l_{c2}	0.75	m
gravity	g	9.8	$\frac{m}{s^2}$

Table 2.1: Design parameters for the two-link planar robot

Because of the point mass approximation of the links, the inertia of the links are taken as $I_1 = 0, I_2 = 0$ and $l_{c1} = l_1, l_{c2} = l_2$.

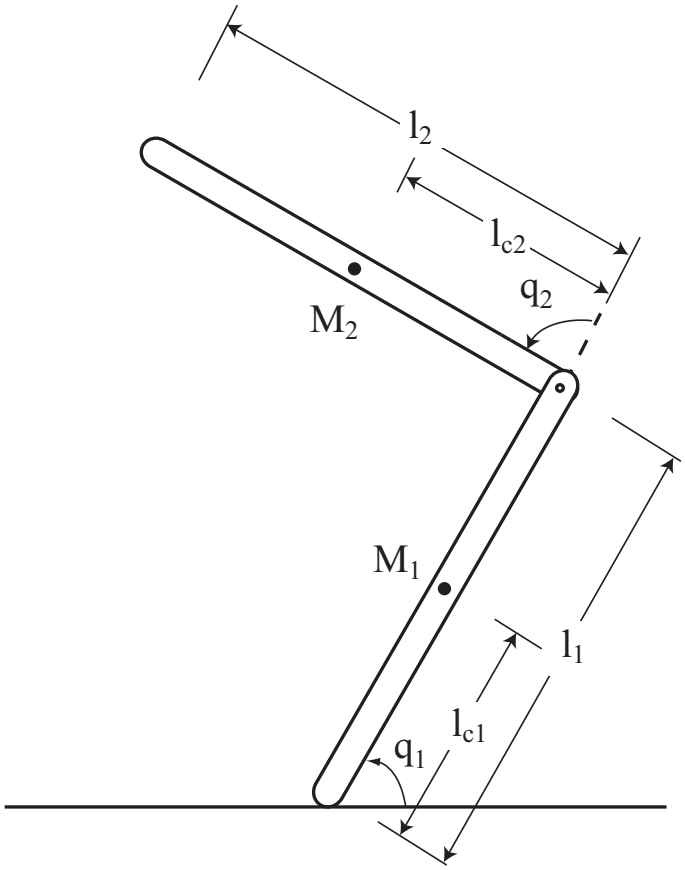

Figure 2.1: The two-link planar robot: parameters and configuration variables.

2.4.1 Configuration Variables

The definition of the parameters, configuration variables and masses of the two-link model are indicated in Figure 2.1. The stance leg angle q_1 is the angle of the stance leg with respect to the ground and the swing leg angle q_2 is the angle of the swing leg with respect to the stance leg. The positive angles are taken in counterclockwise direction. The swing phase of the model is holonomic.

The configuration of the system between the collisions can be defined by two independent generalized coordinates. The state space of the model is four dimensional and the state vector is taken as

$$x = (q_1, q_2, \dot{q}_1, \dot{q}_2)^T. \tag{2.7}$$

The orientation of the model is defined by the Newtonain frame N, stance leg frame A and the swing leg frame B as in Figure 2.2.

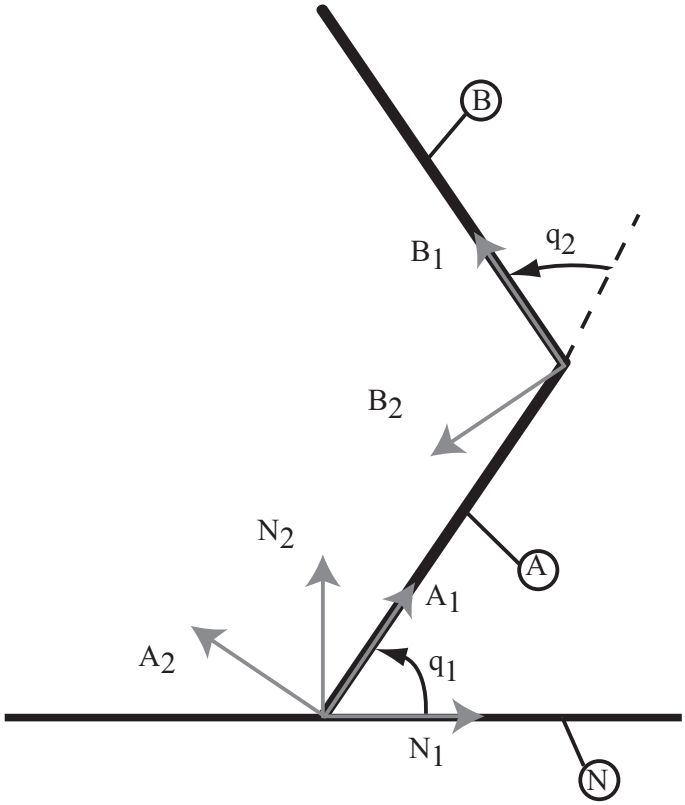

Figure 2.2: Notations for the two-link planar robot indicating the reference frames, bodies points, and basis vectors.

2.4.2 Equations of motion

The second order differential equations of motion during swing phase are given below

$$M(q)\ddot{q} + C(q,\dot{q})\dot{q} + G(q) = Bu, \tag{2.8}$$

where $q = (q_1, q_2)$. The derivation of the equations are presented in Appendix A. The matrices M, C, G and B are calculated as

$$M = \begin{bmatrix} M_1 l_{c1}^2 + I_1 + I_2 + M_2(l_1^2 + 2cos(q_2)l_1 l_{c2} + l_{c2}^2) & I_2 + M_2 l_{c2}(l_{c2} + l_1 cos(q_2)) \\ I_2 + M_2 l_{c2}(l_{c2} + l_1 cos(q_2)) & M_2 l_{c2}^2 + I_2 \end{bmatrix}, \tag{2.9}$$

$$C = \begin{bmatrix} 0 & -M_2 l_1 l_{c2} sin(q_2)\dot{q}_2 - 2M_2 \dot{q}_1 l_1 l_{c2} sin(q_2) \\ M_2 l_1 l_{c2} sin(q_2)\dot{q}_1 & 0 \end{bmatrix}, \tag{2.10}$$

$$G = \begin{bmatrix} gM_2(l_{c2}cos(q_1+q_2) + l_1 cos(q_1)) + gM_1 l_{c1} cos(q_1) \\ gM_2 l_{c2} cos(q_1+q_2) \end{bmatrix}, \tag{2.11}$$

$$B = \begin{bmatrix} 0 \\ 1 \end{bmatrix}. \tag{2.12}$$

2.5 Case Study 2: The three-link planar robot

The robot used in here corresponds to the model presented in [21]. This is a rigid three-link planar robot with revolute joints and two actuators at the hip as shown in Figure 2.3. The parameter values are given in Table 2.2. Because of the point mass

Parameter	Label	Value	Unit
leg mass	M_1	5	kg
leg mass	M_2	5	kg
hip mass	M_h	15	kg
torso mass	M_3	10	kg
leg length	l_1	1	m
leg length	l_2	1	m
torso length	l_3	0.5	m
center of mass length	l_{c1}	0.5	m
center of mass length	l_{c2}	0.5	m
center of mass length	l_{c3}	0.5	m
gravity	g	9.8	$\frac{m}{s^2}$

Table 2.2: Design parameters for the three-link planar robot

approximation of the links, the inertia of the links are taken as $I_1 = 0, I_2 = 0, I_3 = 0$.

The connections between the links are assumed to be implemented by frictionless hinges. The system of links moves on a rigid surface. The stance leg is assumed not to slip due to enough friction with the ground. The motion of the model is governed by the classical laws of rigid body dynamics.

2.5.1 Configuration Variables

The definition of the parameters, configuration variables and masses of the three-link model are indicated in Figure 2.3. q_1 parameterizes the stance leg, q_2 the swing leg, and q_3 the torso. The positive angles are taken in counterclockwise direction.

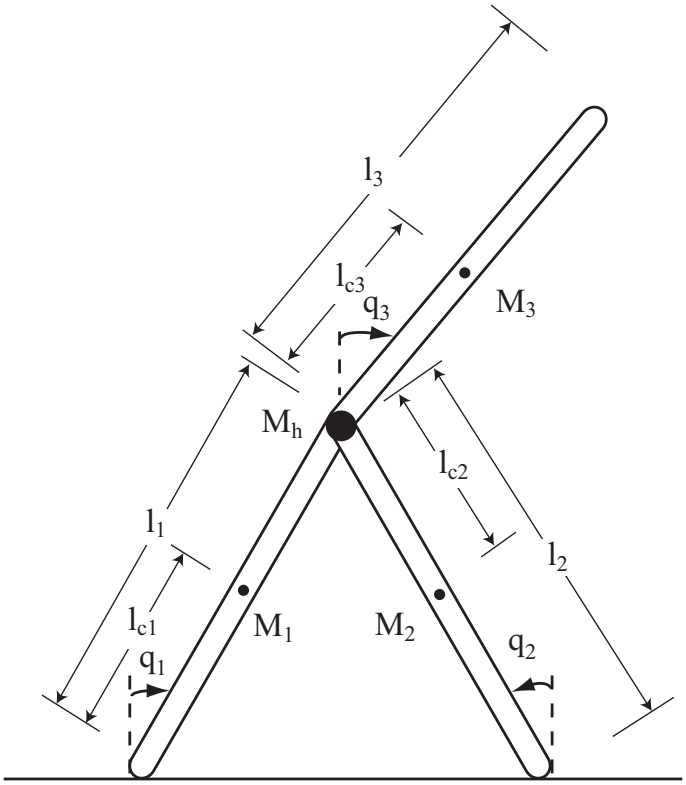

Figure 2.3: The three-link planar robot: parameters and configuration variables.

The swing phase of the model is holonomic. The position between the collisions is defined by three generalized coordinates. The state space of the model is six dimensional and the state vector is taken as

$$x = (q_1, q_2, q_3, \dot{q}_1, \dot{q}_2, \dot{q}_3)^T. \tag{2.13}$$

The orientation of model is defined by the Newtonian frame N, stance leg frame A, the swing leg frame B and the torso frame C as in Figure 2.4.

2.5.2 Equations of motion

The second order differential equations of motion during swing phase is given below

$$M(q)\ddot{q} + C(q, \dot{q})\dot{q} + G(q) = Bu, \tag{2.14}$$

where $q = (q_1, q_2, q_3)$. The derivation of the equations is detailed in Appendix A. The matrices M, C, G and B are calculated as

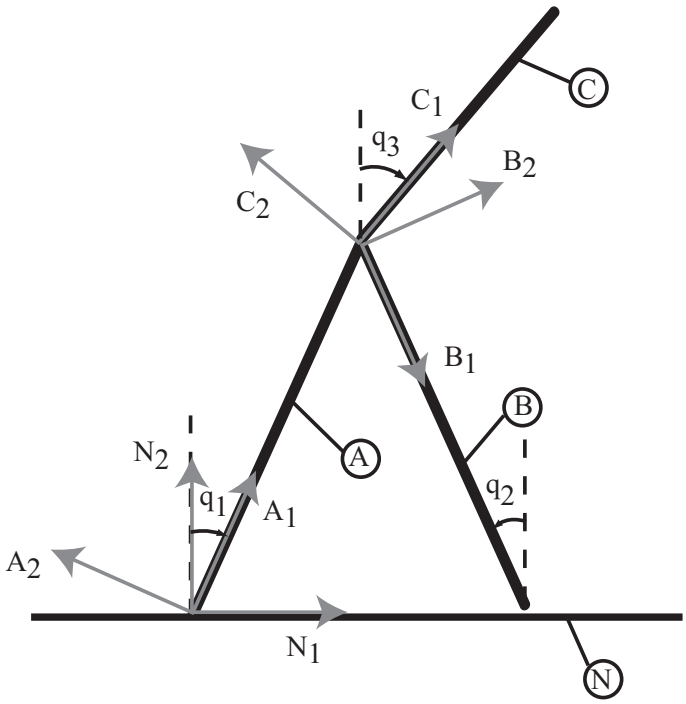

Figure 2.4: Notations for the three-link planar robot indicating the reference frames, bodies, points and basis vectors.

$$M = \begin{bmatrix} I_1 + M_2 l_1^2 + M_3 l_1^2 + M_1 l_{c1}^2 + M_h l_1^2 & -M_2 l_1 l_{c2} cos(q_1 - q_2) & M_3 l_1 l_{c3} cos(q_1 - q_3) \\ -M_2 l_1 l_{c2} cos(q_1 - q_2) & M_2 l_{c2}^2 + I_2 & 0 \\ M_3 l_1 l_{c3} cos(q_1 - q_3) & 0 & M_3 l_{c3}^2 + I_3 \end{bmatrix}, \tag{2.15}$$

$$C = \begin{bmatrix} 0 & -l_1 M_2 \dot{q}_2 l_{c2} sin(q_1 - q_2) & -l_1 M_3 \dot{q}_3 l_{c3} sin(q_1 - q_3) \\ M_2 l_1 l_{c2} sin(q_1 - q_2)\dot{q}_1 & 0 & 0 \\ -M_3 l_1 l_{c3} sin(q_1 - q_3)\dot{q}_1 & 0 & 0 \end{bmatrix}, \tag{2.16}$$

$$G = \begin{bmatrix} -M_2 g l_1 sin(q_1) - M_3 g l_1 sin(q_1) - M_1 g l_{c1} sin(q_1) - M_h g l_1 sin(q_1) \\ M_2 g l_{c2} sin(q_2) \\ -M_3 g l_{c3} sin(q_3) \end{bmatrix}, \tag{2.17}$$

$$B = \begin{bmatrix} -1 & 0 \\ 0 & -1 \\ 1 & 1 \end{bmatrix}. \tag{2.18}$$

2.5.3 Impact

An impact occurs when the geometric impact conditions are satisfied such that

$$q_1 = q_1^d \tag{2.19}$$

$$h = l_1 cos(q_1) - l_2 cos(q_2) = 0 \tag{2.20}$$

where q_1^d is the desired stance angle and h is the distance of the swing leg end from ground. When the swing leg collides with the ground stance leg switches to the swing leg and the legs reset at each impact

$$\begin{bmatrix} q_1^+ \\ q_2^+ \\ q_3^+ \end{bmatrix} = s \begin{bmatrix} q_1^- \\ q_2^- \\ q_3^- \end{bmatrix}, \qquad \text{where} \quad s = \begin{bmatrix} 0 & 1 & 0 \\ 1 & 0 & 0 \\ 0 & 0 & 1 \end{bmatrix}. \tag{2.21}$$

According to the notation, the '+' superscript means 'after impact' and '-' superscript means 'before impact'.

The swing foot receives an impulse when impact occurs and this impulse is also transmitted to the swing leg at the hip joint. The swing leg does not slip or rebound during the impact. During the impact, the other forces such as gravity are considered to be smaller with respect to the impulsive forces and are neglected. Additionally, no impulsive ground contact torques act and the actuators can not generate impulses. These assumptions imply that the total angular momentum is conserved [28] for the entire system about the swing leg contact point. Angular momentum is also conserved for the new swing leg and torso about the hip joint. Referring to Figure B.1, the conservation equations for the entire system is

$$H_E^- = H_E^+ \tag{2.22}$$

and for the new swing leg and torso is

$$H_H^- = H_H^+. \tag{2.23}$$

The conservation equations are explained in detail in Appendix B and are given as

$$Q^+ \begin{bmatrix} \dot{q}_1^+ \\ \dot{q}_2^+ \\ \dot{q}_3^+ \end{bmatrix} = Q^- \begin{bmatrix} \dot{q}_1^- \\ \dot{q}_2^- \\ \dot{q}_3^- \end{bmatrix} \tag{2.24}$$

where Q^+ and Q^- are presented in Appendix B.

Chapter 3

Set Point Control

The adopted mechanical systems demonstrate complex internal dynamics and inherent underactuation which restricts full-state linearization. Some commonly used methods for nonlinear control design include backstepping [29], sliding mode control [32], feed forwarding [35], and high-gain methods [35]. However, these methods usually are not directly applicable to the underactuated systems due to the lack of any method, that transforms the underactuated systems into cascade nonlinear forms with triangular and nontriangular structures.

In [51], [52], Spong showed that partial feedback linearization can be used for controlling either configuration variable of the underactuated mechanical system Acrobot. By a suitable nonlinear feedback, partially linear response can be achieved on this system. Linearization of the unactuated configuration dynamic can be achieved with the method called noncollocated partial feedback linearization [51].

In this chapter, the commonly used underactuated system example, Acrobot is studied to illustrate the underactuation problem. Acrobot is a planar robot with revolute joints and one actuator at the second joint which makes the system underactuated because there is less actuation than its configuration variables. Thus, Acrobot dynamics are not feedback linearizable with static state feedback and nonlinear coordinate transformation. In order to control Acrobot dynamics, set-point control method is designed. The control task is to stabilize the Acrobot at the unstable upright position from an initial condition. The task covers swinging up the two-link robot from an initial position and bringing the links close to their inverted equilibrium condition. Then, the controller switches to a linear controller to balance the system around this position where the robot can be locally asymptotically

stabilized. The defined task will be achieved by first partially linearizing the system with feedback and then the system will switch to a linear controller near upright equilibrium as the system gets into the basin of attraction of the linear controller.

3.1 Partial feedback linearization of a two-link planar robot

In this chapter, the two-link robot with two degrees of freedom as a simple example of an underactuated system is studied. The dynamic model of the robot is explained in Section 2.4. The equations of motion of the system can be rewritten as follows

$$M_{11}\ddot{q}_1 + M_{12}\ddot{q}_2 + C_1 + G_1 = 0 \tag{3.1}$$

$$M_{21}\ddot{q}_1 + M_{22}\ddot{q}_2 + C_2 + G_2 = u \tag{3.2}$$

where

$$C_1 = C_{11}\dot{q}_1 + C_{12}\dot{q}_2 \tag{3.3}$$

$$C_2 = C_{21}\dot{q}_1 + C_{22}\dot{q}_2. \tag{3.4}$$

In order to apply partial feedback linearization, $\ddot{q}_2$ is solved for from (3.1) and replaced in equation (3.2) so that the second equation will be feedback linearizable for $\ddot{q}_1$

$$\ddot{q}_2 = -\frac{1}{M_{12}}(M_{11}\ddot{q}_1 + C_{11}\dot{q}_1 + C_{12}\dot{q}_2 + G_1) \tag{3.5}$$

assuming that M_{12} is nonzero for all values of q_2. Substituting $\ddot{q}_2$ into (3.2) the following is obtained

$$\bar{M}\ddot{q}_1 + \bar{C} + \bar{G} = u \tag{3.6}$$

where

$$\bar{M} = M_{21} - \frac{M_{22}M_{11}}{M_{12}} \tag{3.7}$$

$$\bar{C} = C_2 - \frac{M_{22}C_1}{M_{12}} \tag{3.8}$$

$$\bar{G} = G_2 - \frac{M_{22}G_1}{M_{12}}. \tag{3.9}$$

Therefore, the feedback linearizing controller can be designed as follows

$$u = \bar{M}\nu + \bar{C} + \bar{G}, \tag{3.10}$$

resulting in linear system dynamics of

$$\ddot{q}_1 = \nu. \tag{3.11}$$

A linear controller is designed as

$$\nu = \ddot{q}_1^d - K_d(\dot{q}_1 - \dot{q}_1^d) - K_p(q_1 - q_1^d), \tag{3.12}$$

where ν is the input term with q_1^d as the desired angle, K_p and K_d are the positive gains and $\ddot{q}_1^d$ and $\dot{q}_1^d$ are set to zero for set-point tracking.

With partial feedback linearization, the first link angle is decoupled from the second link angle and the desired input is obtained while the second link oscillates around the equilibrium point. The dynamics of the second link is crucial in order to realize the oscillations. By substituting the reference variables $q_1 = \frac{\pi}{2}$, $\dot{q}_1 = 0$, and $\ddot{q} = 0$ into the equation (3.1), the following equation is obtained

$$\ddot{q}_2 = -(g l_{c2} M_2 \cos(\frac{\pi}{2} + q_2) - l_1 l_{c2} M_2 \dot{q}_2^2 \sin(q_2))/(I_2 + l_{c2} M_2 (l_{c2} + l_1 \cos(q_2))) \tag{3.13}$$

which has its equilibrium points at $(0, 0)$, $(\pi, 0)$. The oscillations take place around these points depending on the tuning of the gains.

3.2 Linear control law

After achieving the steady state behavior for the first link and the second link gets close to the desired upright equilibrium point, the system switches from the nonlinear controller to the linear controller in order to stabilize the second link around the unstable inverted equilibrium point. The two-link system is linearized around the upright equilibrium point $x = 0$ to obtain a controllable linear system

$$\dot{x} = Ax + Bu \tag{3.14}$$

with the state vector $x = (q_1 - q_1^d, q_2, \dot{q}_1, \dot{q}_2)$ and control input u. The A and B matrices are

$$A = \begin{bmatrix} 0 & 0 & 1 & 0 \\ 0 & 0 & 0 & 1 \\ 19.6000 & -19.6000 & 0 & 0 \\ -19.6000 & 45.7333 & 0 & 0 \end{bmatrix}, \tag{3.15}$$

$$B = \begin{bmatrix} 0 \\ 0 \\ -0.9524 \\ 1.8413 \end{bmatrix}. \tag{3.16}$$

For this problem, the reference angle is set as $q_1^d = \frac{\pi}{2}$ and the state feedback is assigned as $u = Kx$.

The linear approximation of the system depends on the pair (A, B) to be controllable. In that case, the linear approximation is asymptotically stabilizable and $A+BK$ has all eigenvalues with negative real part where the feedback asymptotically stabilizes the nonlinear system. The poles of the linearized open-loop system are at $-7.4982, -3.0183, 7.4982, 3.0183$, showing that the equilibrium position is unstable.

A linear quadratic regulator (LQR), that is an optimal state-feedback controller that minimizes the quadratic cost criterion,

$$J = \int_0^\infty (\mathbf{x}^T Q \mathbf{x} + \tau^T R \tau) dt \tag{3.17}$$

is designed to move the poles to the stable region. The matrices Q and R are used to weight the states and the input in the cost function. The LQR is designed with the weighting matrices

$$Q = \begin{bmatrix} 1 & 0 & 0 & 0 \\ 0 & 1 & 0 & 0 \\ 0 & 0 & 1 & 0 \\ 0 & 0 & 0 & 1 \end{bmatrix} \tag{3.18}$$

$$R = [1]. \tag{3.19}$$

The corresponding state-feedback, K, values are

$$K = [-1360.7 - 438.9 - 583.2 - 215.5]. \tag{3.20}$$

The poles of the linearized system are placed at $-8.5979, -6.5436, -3.0322, -3.0045$. With the designed state feedback, the system can be stabilized at the inverted equilibrium point.

3.3 Simulation results

The two-link robot model is simulated in Matlab. The nonlinear equations of motion are integrated with the ode45 function, a $4th - 5th$ order automatic step-

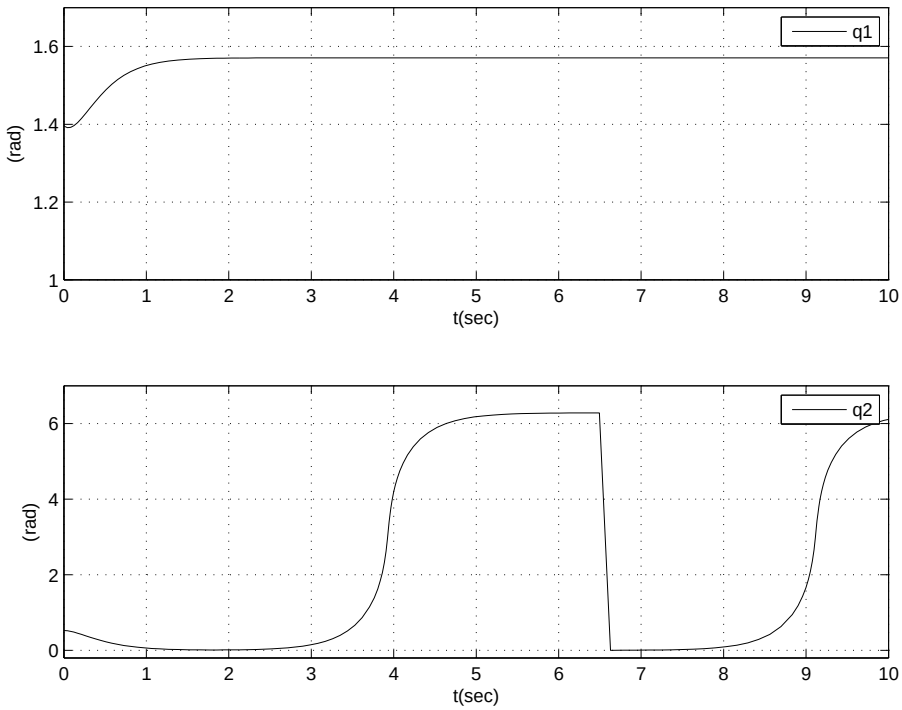

Figure 3.1: The simulation results of the two-link robot for the joint angles q_1 and q_2 versus time. q_1 sets to the desired position $q_1^d = \pi/2$ and q_2 oscillates around the equilibrium point.

sizing routine. An integration tolerance of 10^{-5} is used.

The response of the partial feedback controller can be observed from the Figure 3.1 where the first link converges to the desired configuration and the second link oscillates around its equilibrium point $(\pi, 0)$. The second link's trajectory is plotted as module 2π which resulted in jumps in the figure.

The inverted equilibrium state space for the two-link robot is $x = (\frac{\pi}{2}, 0, 0, 0)$. The controller is switched to the balancing controller when the pendulum is brought near the inverted equilibrium point such that $q_2 < \frac{\pi}{6}$. Figures 3.2 and 3.3 show the simulation results of swinging up and balancing with partial feedback linearization and then with state feedback around the equilibrium. Tuning of the LQR gains is crucial for obtaining the desired motion as the linear approximation has a small basin of attraction. The positive gains of the nonlinear feedback controller are tuned as $K_p = 16$ and $K_d = 8$. The simulation results demonstrate a set-point control method for the underactuated system where the angular coordinates converge to the desired positions and the angular velocities become zero.

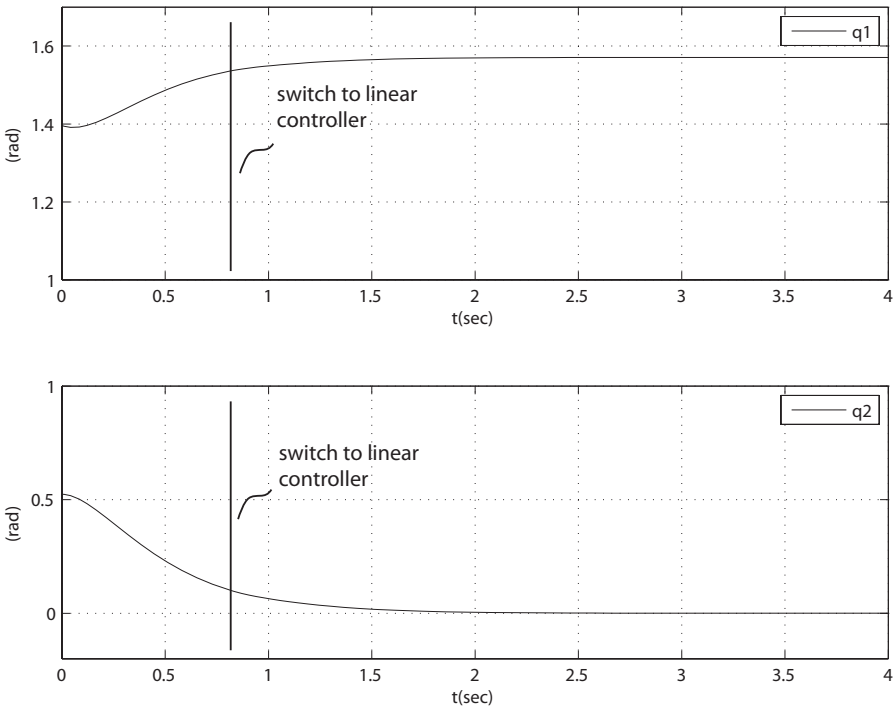

Figure 3.2: The simulation results of the two-link robot for the joint angles q_1 and q_2 versus time. q_1 sets to the desired position $q_1^d = \pi/2$ and q_2 converges to zero.

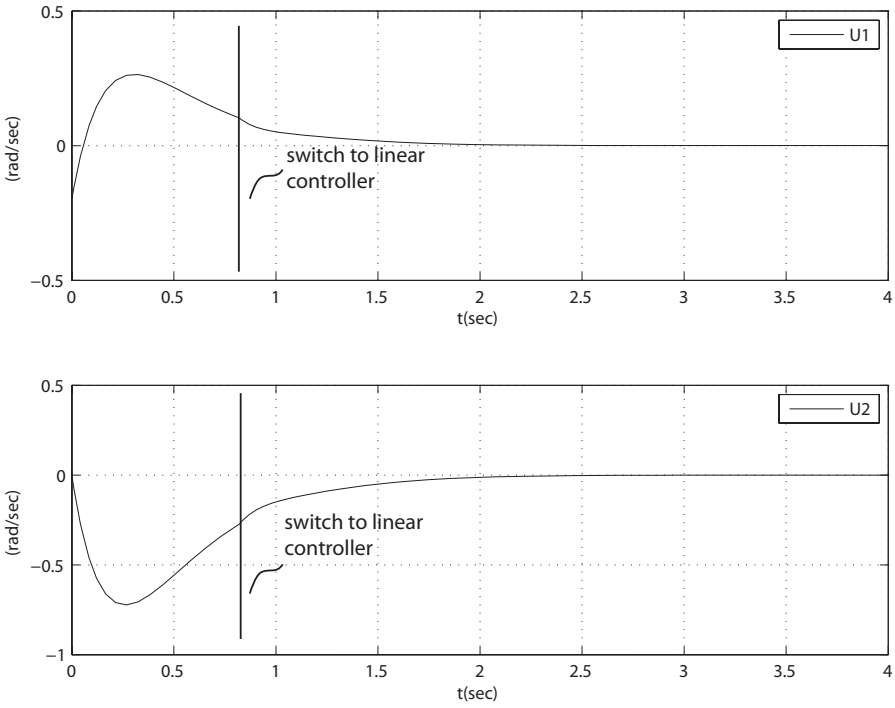

Figure 3.3: The simulation results of the two-link robot for the joint velocities $\dot{q}_1$ and $\dot{q}_2$. Both $\dot{q}_1$ and $\dot{q}_2$ converge to zero.

Chapter 4

Trajectory Tracking Control

In this chapter, the trajectory tracking control method is investigated to realize dynamic motions in underactuated systems with a control design procedure for achieving a continuous trajectory via assigning a set of outputs to zero. When these outputs are identically zero, the resulting dynamics of the system are called the zero dynamics. The analysis of zero dynamics is crucial to the understanding of the behavior of the complete system.

In Chapter 3, a set-point controller is obtained by switching between the swing up and balancing controllers. In the set-point control method, the task is the asymptotic convergence to an equilibrium point which has its drawback on demonstrating poor performance in terms of time (slow) and it lacks tracking periodic orbits to reach dynamically balanced motions. This initiated designing a controller that motivates tracking closed-loop motions by coordinating the relation among the configuration variables.

In the trajectory tracking controller, a feedback is designed to track time-invariant trajectories only depending on the system states. A set of outputs are defined and imposed on the system by the feedback controller where the control input partially linearizes the system. The resulting dynamics of the system are called the zero dynamics which can be shaped according to the choice of the outputs. Imposing the outputs on the system is restricting the system to move in the determined path such that the system is in a sense virtually constrained. The shaped zero dynamics is used to observe the stability of the complete system. The trajectory tracking controller is covered by considering the two-link planar robot, Acrobot.

4.1 Zero dynamics

In input-output feedback linearization method, a set of outputs equal in number with the inputs are defined and the feedback controller asymptotically drives the outputs to zero. These outputs can consist of holonomic constraints which are parameterized by the system states. Imposing the set of outputs encodes the robot's task such that nulling of these is equivalent to achieving the desired task. When the outputs are identically zero, the internal dynamics of the system is called the zero dynamics [29]. Because in underactuated systems the dimension of the zero dynamics is less than the dimension of the model, the robot task is implicitly encoded into a lower dimensional system. The notation is taken from [29].

Consider a nonlinear system

$$\dot{x} = f(x) + g(x)u \tag{4.1}$$

$$y = h(x) \tag{4.2}$$

with n degrees of freedom and r relative degree which is the number of times the output is differentiated to reach the input explicitly. With the introduction of local coordinate transformation, the system is transformed into a cascade nonlinear system. Then, a proper state feedback is designed to linearize this system. If for example $r < n$ for the given output, rather then exact linearization, the system is partially linearized. By defining the new coordinates the nonlinear system becomes

$$\begin{aligned} y &= z_1 && (4.3)\\ \dot{z}_1 &= z_2 \\ \dot{z}_2 &= z_3 \\ &\cdots \\ \dot{z}_{r-1} &= z_r \\ \dot{z}_r &= b(z) + a(z)u && (4.4)\\ \dot{z}_{r+1} &= q_1(z) + p_1(z)u \\ &\cdots \\ \dot{z}_n &= q_{n-r}(z) + p_{n-r}(z)u. \end{aligned}$$

With a state feedback, the system is turned into a partially linear model where the

nonlinear part does not affect the output. Define the new state vectors

$$\xi = \begin{pmatrix} z_1 \\ \cdots \\ z_r \end{pmatrix}, \tag{4.5}$$

$$\eta = \begin{pmatrix} z_{r+1} \\ \cdots \\ z_n \end{pmatrix}. \tag{4.6}$$

The output is forced to be zero which implies $\xi = 0$, and

$$0 = b(\xi, \eta) + a(\xi, \eta)u \tag{4.7}$$

with the feedback

$$u = -\frac{b(\xi, \eta)}{a(\xi, \eta)}. \tag{4.8}$$

The zero dynamics of the system is described as

$$\dot{\eta} = q(0, \eta) - p(0, \eta)\frac{b(0, \eta)}{a(0, \eta)}. \tag{4.9}$$

The dynamics turn into the partially linear system

$$\dot{\xi} = A\xi \tag{4.10}$$

$$\dot{\eta} = q(\xi, \eta) + p(\xi, \eta)u \tag{4.11}$$

$$y = C\xi, \tag{4.12}$$

where

$$A = \begin{bmatrix} 0 & 1 & 0 & \cdots & 0 \\ 0 & 0 & 1 & \cdots & 0 \\ . & . & . & \cdots & . \\ 0 & 0 & 0 & \cdots & 1 \\ 0 & 0 & 0 & 0 & 0 \end{bmatrix}$$

$$C = \begin{bmatrix} 1 & 0 & 0 & \cdots & 0 \end{bmatrix}. \tag{4.13}$$

4.2 Swing phase zero dynamics

In order to construct feedback controllers for the presented robots, swing phase zero dynamics are defined in the original coordinates. The output $y = h(x)$ depends

only on the configuration variables. But its derivative does not depend directly on the inputs due to the second order nature of the robots.

Given the state vector is $x = (q, \dot{q})$.

$$\frac{dy}{dt} = \frac{\partial h}{\partial x}\dot{x} \tag{4.14}$$

$$= \begin{bmatrix} \frac{\partial h}{\partial q} & \frac{\partial h}{\partial \dot{q}} \end{bmatrix} \left\{ \begin{bmatrix} \dot{q} \\ M^{-1}[-C\dot{q} - G] \end{bmatrix} + \begin{bmatrix} 0 \\ M^{-1}B \end{bmatrix} u \right\} \tag{4.15}$$

$$= \begin{bmatrix} \frac{\partial h}{\partial q} & 0 \end{bmatrix} \begin{bmatrix} \dot{q} \\ M^{-1}[-C\dot{q} - G] \end{bmatrix} + \begin{bmatrix} \frac{\partial h}{\partial q} & 0 \end{bmatrix} \begin{bmatrix} 0 \\ M^{-1}B \end{bmatrix} u \tag{4.16}$$

$$= L_f h(x) \tag{4.17}$$

$L_g h(x) = 0$ so it is differentiated again.

$$\frac{d^2y}{dt^2} = \begin{bmatrix} \frac{\partial}{\partial q}(\frac{\partial h}{\partial q}\dot{q}) & \frac{\partial h}{\partial q} \end{bmatrix} \left\{ \begin{bmatrix} \dot{q} \\ M^{-1}[-C\dot{q} - G] \end{bmatrix} + \begin{bmatrix} 0 \\ M^{-1}B \end{bmatrix} u \right\} \tag{4.18}$$

$$= \begin{bmatrix} \frac{\partial}{\partial q}(\frac{\partial h}{\partial q}\dot{q}) & \frac{\partial h}{\partial q} \end{bmatrix} \begin{bmatrix} \dot{q} \\ M^{-1}[-C\dot{q} - G] \end{bmatrix} + \frac{\partial h}{\partial q} M^{-1} B u \tag{4.19}$$

$$= L_f^2 h(q) + L_g L_f h(q) u \tag{4.20}$$

It is assumed then, that the matrix $L_g L_f h(q)$ is invertible to have the existence and uniqueness property of the zero dynamics [29]. It is also assumed that $L_g L_f h(q)$ is square and invertible for the given open set.

Then, the zero dynamics manifold is defined as

$$Z = \{x \in \mathbb{R}^n : h(x) = L_f h(x) = 0\} \tag{4.21}$$

and the feedback

$$u(x) = -(L_g L_f h(x))^{-1} L_f^2 h(x) \tag{4.22}$$

is applied to render Z invariant under the zero dynamics manifold.

4.3 Stabilization

In this section, a locally stabilizing feedback for the nonlinear model will be defined. The nonlinear control law is also given in [29]. The zero dynamics are locally asymptotically stabilized at equilibrium $(\xi, \eta) = (0, 0)$.

Setting the state feedback to

$$u = \frac{1}{a(z)}(-b(z) + \nu), \tag{4.23}$$

the new equations become

$$\begin{aligned} y &= z_1 \\ \dot{z}_1 &= z_2 \\ \dot{z}_2 &= z_3 \\ &\cdots \end{aligned} \tag{4.24}$$

$$\begin{aligned} \dot{z}_{r-1} &= z_r \\ \dot{z}_r &= \nu \\ &\cdots \\ \dot{\eta} &= q(z) + p(z)u \end{aligned} \tag{4.25}$$

selecting

$$\nu = -k_0 z_1 - k_2 z_2 - \cdots - k_{r-1} z_r \tag{4.26}$$

with $k_0, \ldots, k_{r-1}$ are positive real numbers. The closed loop system becomes

$$\begin{aligned} \dot{\xi} &= A\xi \\ \dot{\eta} &= Q(\xi, \eta), \end{aligned} \tag{4.27}$$

with

$$A = \begin{bmatrix} 0 & 1 & 0 & \cdots & 0 \\ 0 & 0 & 1 & \cdots & 0 \\ . & . & . & \cdots & . \\ 0 & 0 & 0 & \cdots & 1 \\ -k_0 & -k_1 & -k_2 & \cdots & -k_{r-1} \end{bmatrix}. \tag{4.28}$$

The matrix A has the characteristic polynomial

$$p(s) = k_0 + k_1 s + \cdots + k_{r-1} s^{r-1} + s^r. \tag{4.29}$$

When the equilibrium point $\eta = 0$ of the zero dynamics is locally asymptotically stable and the roots of the polynomial have negative real part then the feedback law locally asymptotically stabilizes the equilibrium $(\xi, \eta) = (0, 0)$.

4.4 Case study: Two-link planar robot

This section presents the feedback controller for the two-link planar robot. The equations of motion of the two-link planar robot are stated in Section 2.4 and derived in Appendix A.

Virtual Constraints

This part develops the virtual constraints for the two-link planar robot to have periodic motions. For the desired trajectory q_1 and q_2 express the desired motion. Instead of setting the system to an equilibrium point, it is enforced to oscillate around the equilibrium point. The simplest way to achieve this is to relate these to each other so that the motion is symmetric around the equilibrium point.

The virtual constraint that is enforced on the system is selected as

$$y = 2q_1 + q_2 - \pi. \tag{4.30}$$

Following the procedure discussed above, the feedback is calculated and fed into the robot to track the desired trajectory. Since the system has relative degree of two, the output is differentiated twice. The input is derived as

$$u = \left(\frac{\partial h(q)}{\partial q} M^{-1} B\right)^{-1} \left(\frac{\partial h(q)}{\partial q} M^{-1}(C\dot{q} + G) - \frac{\partial}{\partial q}(\frac{\partial h(q)}{\partial q})\dot{q}^2\right) \tag{4.31}$$

where the M, C, G and B matrices are given in (2.4.2) and

$$h = 2q_1 + q_2 - \pi \tag{4.32}$$

$$\frac{\partial h(q)}{\partial q} = 2\dot{q}_1 + \dot{q}_2 \tag{4.33}$$

$$\frac{\partial}{\partial q}(\frac{\partial h(q)}{\partial q}) = 0. \tag{4.34}$$

Controller

The system is transformed into cascade form, to study the stabilizing dynamics of the output. The local coordinate transformation is defined as

$$\xi_1 = y$$

$$\xi_2 = \dot{y}$$

$$\eta_1 = q_2$$

$$\eta_2 = \dot{q}_2,$$

where the closed loop equations become

$$\dot{\xi}_1 = \xi_2 \tag{4.35}$$

$$\dot{\xi}_2 = \nu \tag{4.36}$$

$$\dot{\eta}_1 = \eta_2 \tag{4.37}$$

$$\dot{\eta}_2 = P(\xi, \eta). \tag{4.38}$$

Thus, the system is transformed into cascade form. With the feedback

$$u = (L_g L_f h(x))^{-1}(\nu - L_f^2 h(x)), \tag{4.39}$$

the surface $\xi = 0$ becomes an invariant manifold for the system. Because of the enforced output, $q_1 = \frac{\pi - q_2}{2}$, $\dot{q}_1 = \frac{-\dot{q}_2}{2}$ and $\ddot{q}_1 = \frac{-\ddot{q}_2}{2}$. Substituting these into $P(\xi, \eta)$ results in $\dot{\eta}_2 = (2gl_{c1}M_1 \sin(\frac{q_2}{2}) + 2gl_1 M_2 \sin(\frac{q_2}{2}) + 2gl_{c2}M_2 \sin(\frac{q_2}{2}))/(M_2 l_1^2 + M_1 l_{c1}^2 - M_2 l_{c2}^2 + I_1 - I_2)$.

The feedback is imposed on the system so that the system is locally asymptotically stabilized. The stabilizing control law is in the form

$$\nu = -k_0 \xi_1 - k_1 \xi_2. \tag{4.40}$$

The linear feedback gains are chosen as $k_0 = 10, k_1 = 1$. The stability of the zero dynamics is analyzed by studying the behavior of zero dynamics $\dot{\eta} = Q(\xi, \eta)$ around the equilibrium point $\eta = 0$.

$$\dot{\eta} = \frac{\partial Q(\xi, \eta)}{\partial \eta}|_{(\xi,\eta)=(0,0)} \tag{4.41}$$

has its eigenvalues at $(6.2610i, -6.2610i)$ which shows that the chosen equilibrium point is a center. This shows that the system is locally asymptotically stabilized with the given feedback.

Simulation results

The two-link model is simulated and the nonlinear equations of motion are integrated with a $4th - 5th$ order automatic step-sizing Runge-Kutta routine. An integration tolerance of 10^{-5} is used. The initial conditions for the two-link robot

are defined as

$$q_1 = \frac{\pi}{3} \tag{4.42}$$

$$q_2 = \frac{\pi}{3} \tag{4.43}$$

$$\dot{q}_1 = 0 \tag{4.44}$$

$$\dot{q}_2 = 0. \tag{4.45}$$

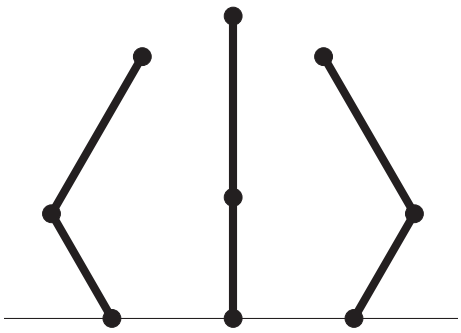

Figure 4.1: Stick figure of the robot shows the constrained motion. The robot starts from the right configuration then moves to the left and oscillates around the upright position.

The stick figure of the robot in Figure 4.1 illustrates the motion of the system. The robot starts from the right configuration and moves to the left. The simulation results of the Acrobot under the imposed control law are presented. In Figure 4.2 the configuration trajectories of the Acrobot are shown where the solid line presents the first link's trajectory and the dashed line is the second link's trajectory. The first link oscillates around $q_1 = \pi/2$ and the second link oscillates around $q_2 = 0$. The Figure 4.3 shows the velocity trajectories of the Acrobot. It is observed that the system oscillates around the desired velocity trajectories. Figure 4.4 shows the configuration trajectories under disturbance. With the outer control loop, the target manifold namely the desired orbit is rendered invariant and system converges to the desired orbit.

Additional to the inverted oscillations, the robot can have trajectories around other set of equilibrium points. The motion of the robot is limited to move around the specific equilibrium conditions because of the chosen physical parameters of the robot. As the parameters are varied new stable trajectories can be obtained and also with the definition of new virtual constrains, different set of orbits can be achieved.

This study has provided a starting point for deriving periodic orbits leading to dynamic walking. The virtual constraints and the control law can be shaped to obtain a walking motion.

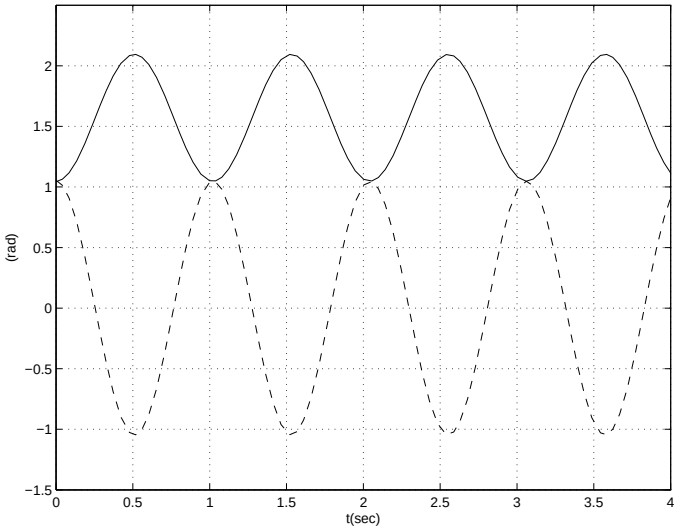

Figure 4.2: The simulation results of the two-link robot showing the joint angles q_1 (straight line) and q_2 (dashed line). The robot is on the desired trajectory which is enforced by the output.

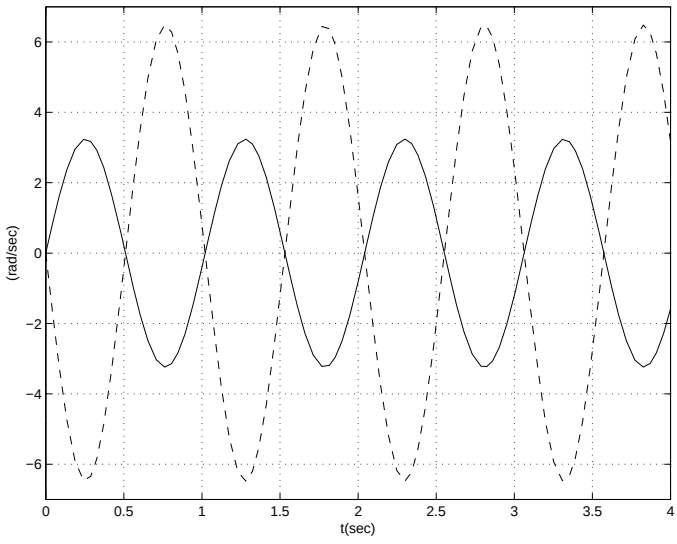

Figure 4.3: The simulation results of the two-link robot showing the joint velocities $\dot{q}_1$ (straight line) and $\dot{q}_2$ (dashed line).

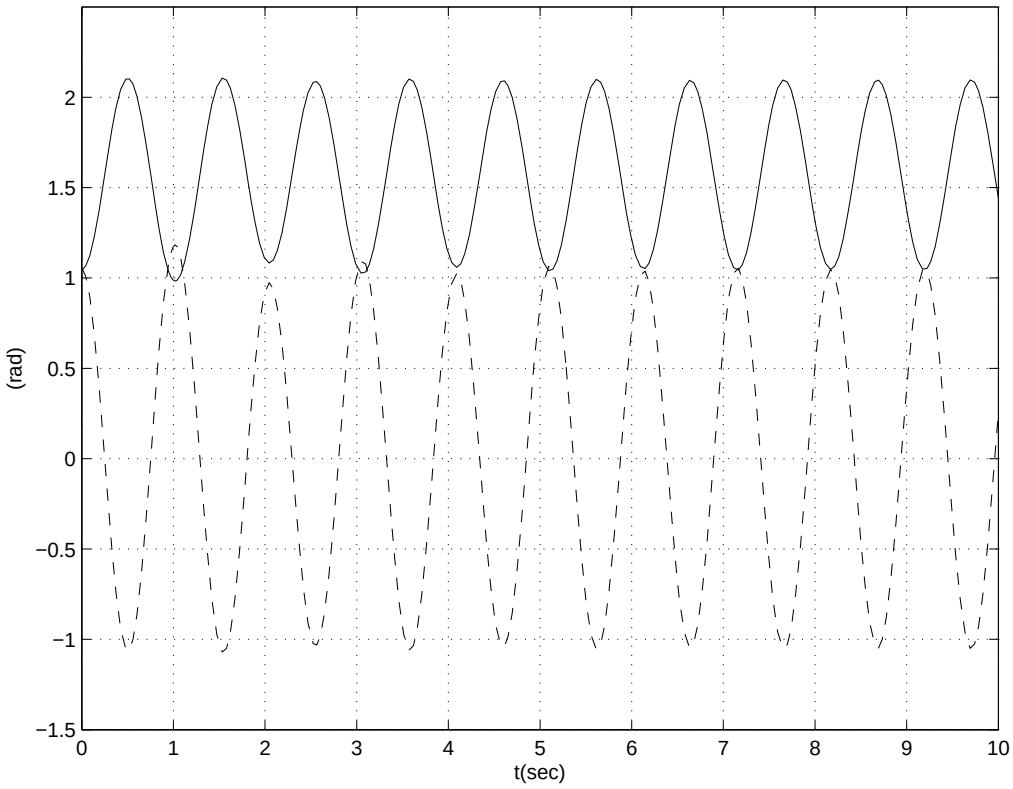

Figure 4.4: The simulation results of the two-link robot showing the joint angles under disturbance $\dot{q}_1$ (straight line) and $\dot{q}_2$ (dashed line).

Chapter 5

Trajectory Tracking Control with Impacts

Walking is a cyclic movement of the legs to translate the body from one place to the next. While the body is balanced on the stance leg, the swing leg moves from the back to forward. This cycle ends with the impact of the swing leg with the ground. The impacts give rise to discrete events where the system becomes piecewise holonomic and in the global case, non-conservative due to the energy loss during inelastic foot collision.

Walking control is similar to the previous study of balancing. In this case, the closed loop dynamics are completed with a discreet impact map. With the trajectory tracking controller, the hybrid system is controlled to achieve the desired periodic behavior of walking. The virtual constraints are designed leading to a stable periodic orbit together with the impact map.

In this section, the two-link model is evolved to simulate human walking considering a additional leg and the impacts with the ground. The analysis of walking mechanism start with the investigation of the multi-link kinematic chain with intermittent contacts. The presented walking robot has two legs and a torso. This dynamic model has been previously studied in literature [59], [21], [62]. The model presented in here is discussed in [21].

The analytical procedure of finding a walking gait can be summarized as follows:

1. The mechanical model is defined. Assumptions are made. Constraints and kinematical descriptions are determined.

2. The equations of motion between the impacts are derived.

3. The impact condition is defined. Then, the reset rule for the states during

impact is derived.

4. The controller is designed to regulate the system trajectory.

5. The dynamical equations are calculated numerically by integrating the equations of motion between impacts until the impact and the impact rule is applied.

6. Validity of the motion is examined to reapply the same procedure with updated parameters and initial conditions until a valid walking motion is achieved.

7. The condition for cyclic motion is imposed and solved for a steady gait.

5.1 Stability analysis: Poincaré map

Walking is a combination of discrete and continuous events and in this sense it is an example of a switching system. In order to study the stability of system's limit cycle, a Poincaré section is used. The Poincaré section S is defined at the impact. The Poincaré map P takes the system from this section to the next section, $P : S \rightarrow S$, meaning that, the mapping P takes the state of the system from just after an impact to the next state just after the impact. The mapping is presented

$$x_{n+1}^{+} = P(x_n^{+}), \tag{5.1}$$

where n corresponds to the step, P to the return map, the '+' signifies just after the impact. In order to have a steady motion, fixed points of the return map should be determined. The periodic motion depends on the fixed points of the return map. x^* corresponds to a fixed point of P if

$$P(x^*) = x^*. \tag{5.2}$$

Periodic motion appears on a Poincaré section with a fixed point.

Fixed point of $P(x^*)$ corresponds to a zero of the function $g(x) = P(x) - x$. When a solution is found, the exponential orbital stability of this solution is determined by finding the analytic Jacobian J of the map P. The Jacobian J is derived numerically by evaluating the return map a number of times in the neighborhood of the fixed point. By studying the the evolution of small perturbations from the fixed point, the

stability of the periodic motions can be examined. The linearization of the return map around the fixed point is given as

$$x^* + \Delta P = P(x^* + \Delta x) \tag{5.3}$$

$$\cong P(x^*) + DP(x^*)\Delta x \tag{5.4}$$

where $DP(x^*) \triangleq J$. Hence, noting x^* is a fixed point, set of linear equations is obtained

$$\Delta x_{n+1} = J\Delta x_n \tag{5.5}$$

where Δ denotes a small deviation from this fixed point. If all the eigenvalues of the Jacobian are strictly inside the unit circle the asymptotic stability can be claimed [23]. Control design exploiting Poincaré map analysis is used in [20], [9] where by using a feedback control law the stability analysis is reduced to a lower dimensional Poincaré map.

5.2 Case study: Three-link planar robot

The equations of motion of the robot are those of a three-link open kinematic chain. Derivations are straightforward and explained in Section 2.5.2. The derivation of the impact condition is given in Section 2.5.3. The complete model of robot in closed form is expressed in Section 2.5.

The procedure to achieve a stable periodic motion is explained as follows:

1. The initial state x_n^+ for the post-impact condition is set, where n corresponds to the number of steps.

2. The virtual constraints and the corresponding feedback controller are defined.

3. The equations of motion are integrated until the impact condition is met resulting in pre-impact state x_n^-.

4. Under the impact function post-impact state x_{n+1}^+ is determined.

5. The new post-impact state is compared with the old post-impact with the error $x_n^+ - x_{n+1}^+ = 0$.

6. In case of error, new initial state is attained until a stable periodic motion is reached.

Virtual Constraints

The swing phase zero dynamics are applied on the three-link planar robot to construct a walking motion. For each actuator a holonomic constraint is defined. The motion of the robot is encoded into the dynamics by defining the outputs with the feedback control which drives the outputs to zero. Driving the outputs to zero enforces the joint angles converge to the desired path.

Commonly, during walking the body is maintained at a desired position, and the swing leg moves from back to forward. Then, the swing leg contacts with the ground. Considering this, the virtual constraints are designed with an intuitive approach. So in the desired walking control, the legs move in symmetric manner and the torso maintains a constant motion [21]. The constraints are taken in the form of the output

$$y = \begin{bmatrix} y_1 \\ y_2 \end{bmatrix} = \begin{bmatrix} q_3 - q_3^d \\ q_2 + q_1 \end{bmatrix}. \tag{5.6}$$

where y_1 regulates the position of the torso by setting to a reference angle and y_2 implies symmetric walking.

Controller

The relative degree of the system with the outputs defined is two as discussed in Section 4.2. After defining the system in partially linear form [29], a feedback controller is imposed on the system. With the feedback controller the system becomes stabilized. The input

$$u = (L_g L_f h(x))^{-1}(\nu - L_f^2 h(x)) \tag{5.7}$$

is fed into the system which results in the double integrator,

$$\ddot{y} = \nu. \tag{5.8}$$

With the addition of impacts, the system becomes hybrid and stability of zero dynamics does not guarantee to achieve a periodic trajectory. After each impact condition, the system needs to stay on the desired trajectory to obtain a stable and periodic motion. So an outer feedback loop needs to be defined to realize periodic motions under impacts. With the definition of outer feedback controllers, finite-

time stabilizing controller [4] and high-gain control, tracking errors are imposed to be zero in finite-time and the errors due to impacts are recovered.

The continuous feedback control law is designed such that finite-time stabilizes the double integrator system

$$\dot{x}_1 = x_2 \tag{5.9}$$

$$\dot{x}_2 = \nu \tag{5.10}$$

is designed as

$$\nu = \psi_a(x_1, x_2) \tag{5.11}$$

$$= -sign(x_2)|x_2|^{\alpha} - sign(\phi_\alpha(x_1, x_2))|\phi_\alpha(x_1, x_2)|^{\frac{\alpha}{2-\alpha}}, \tag{5.12}$$

for all $0 < \alpha < 1$ and $\phi_\alpha(x_1, x_2) = x_1 + \frac{1}{2-\alpha} sign(x_2)|x_2|^{2-\alpha}$. The feedback satisfies that ν is continuous, (5.10) with (5.11) is globally finite-time stable and the time of impact depends on the initial condition. The feedback can be applied to the double integrator such that $\nu = \psi(y, \dot{y})$.

Additionally, the high-gain controller is applied to render the zero dynamics invariant under impact with ϵ that defines a time-scale argument such that for any $\epsilon > 0$ results in high speed disturbance rejection

$$\psi(y, \dot{y}) = \begin{bmatrix} \frac{1}{\epsilon^2}\psi_\alpha(y_1, \epsilon\dot{y}_1) \\ \frac{1}{\epsilon^2}\psi_\alpha(y_2, \epsilon\dot{y}_2) \end{bmatrix}. \tag{5.13}$$

Simulation results

The three-link planar robot is simulated in Matlab and the nonlinear equations of motion are integrated with the ode45 function, a $4th - 5th$ order automatic step-sizing routine. An integration tolerance of 10^{-5} is used. The robot is started from initial condition

$$q_1 = \frac{\pi}{8} \tag{5.14}$$

$$q_2 = -\frac{\pi}{8} \tag{5.15}$$

$$q_3 = -0.9774 \tag{5.16}$$

$$\dot{q}_1 = -1.6 \tag{5.17}$$

$$\dot{q}_2 = 1.6 \tag{5.18}$$

$$\dot{q}_3 = -0.9 \tag{5.19}$$

and integrated until the switching condition

$$S := \{(q, \dot{q}) \in X \mid h = 0, L > 0\} \tag{5.20}$$

is met where

$$h = l_1 cos(q_1) - l_2 cos(q_2) \quad \text{and} \quad L = -l_1 sin(q_1) + l_2 sin(q_2) \tag{5.21}$$

and the desired angle at the impact for the swing leg is $q_1^d = \frac{\pi}{8}$. The feedback is selected as

$$\psi(y, \dot{y}) = \begin{bmatrix} \frac{1}{\epsilon^2}\psi_\alpha(y_1, \epsilon\dot{y}_1) \\ \frac{1}{\epsilon^2}\psi_\alpha(y_2, \epsilon\dot{y}_2) \end{bmatrix} \tag{5.22}$$

with $\epsilon = 0.1$ and $\alpha = 0.9$, as proposed in the literature [21]. The finite-time convergence controller and high gain controller are combined to form the control law to ensure that the periodic motions occur in finite time.

The fixed point of this motion is found at

$$x^* = [\ \tfrac{\pi}{8} \quad -\tfrac{\pi}{8} \quad -0.9774 \quad -1.6 \quad 1.6 \quad -0.9\ ]. \tag{5.23}$$

The computed eigenvalues of the linearized Poincaré map are

$$\sigma = [\ 1 \quad 0.5492 \quad -0.0027 \quad 0 \quad 0 \quad 0\ ]. \tag{5.24}$$

If the eigenvalues have magnitude less than 1, the orbit corresponding to the fixed point is locally asymptotically stable. When one of the eigenvalues is exactly equal to one and rest of them have magnitude strictly less than one, the periodic motion is asymptotically stable. That is, under small disturbance the system can exponentially converge to a nearby periodic motion.

The stick figure of the robot shown in Figure 5.1 illustrates the motion of the system for one step. The model's angular coordinates for the leg trajectories over 3 steps are illustrated in Figure 5.2. The solid line represents the first link's trajectory and the dashed line represents the second link's trajectory. The straight lines in the configuration coordinates correspond to the impact condition. The Figure 5.3 shows the trajectory of the torso. In the Figure 5.4, the angular velocities of the legs for 3 steps are illustrated. The solid line corresponds to the stance leg's trajectory while the dashed line corresponds to the swing leg's trajectory. The instantaneous velocity changes happen while the positions remain the same. The phase portrait

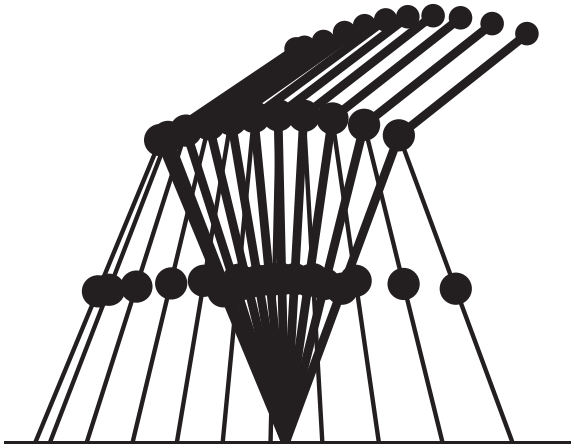

Figure 5.1: Stick figure of the robot.

of the stance leg is shown in Figure 5.6. It is seen that the trajectory converges to the orbit. If the robot starts slightly away from its limit cycle, it will converge to the limit cycle within a few steps.

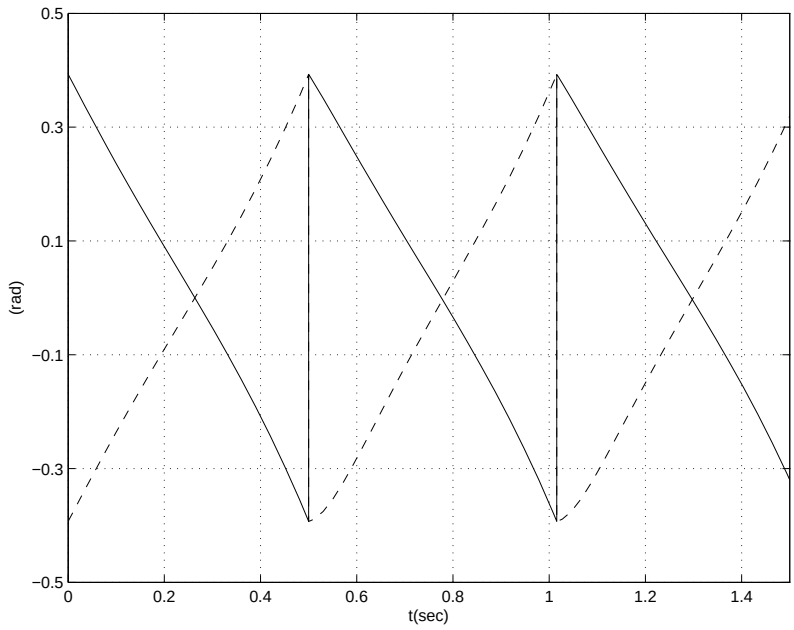

Figure 5.2: The simulation result of the robot showing the leg angles q_1 (straight line) and q_2 (dashed line) versus time for 3 steps. The straight lines corresponds to the impacts.

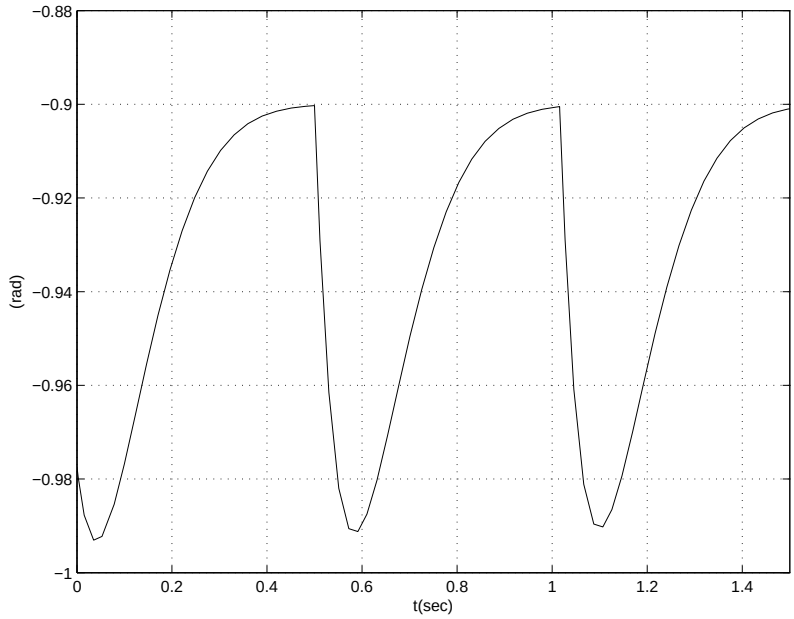

Figure 5.3: The simulation result of the robot showing the torso angle q_3 versus time for 3 steps.

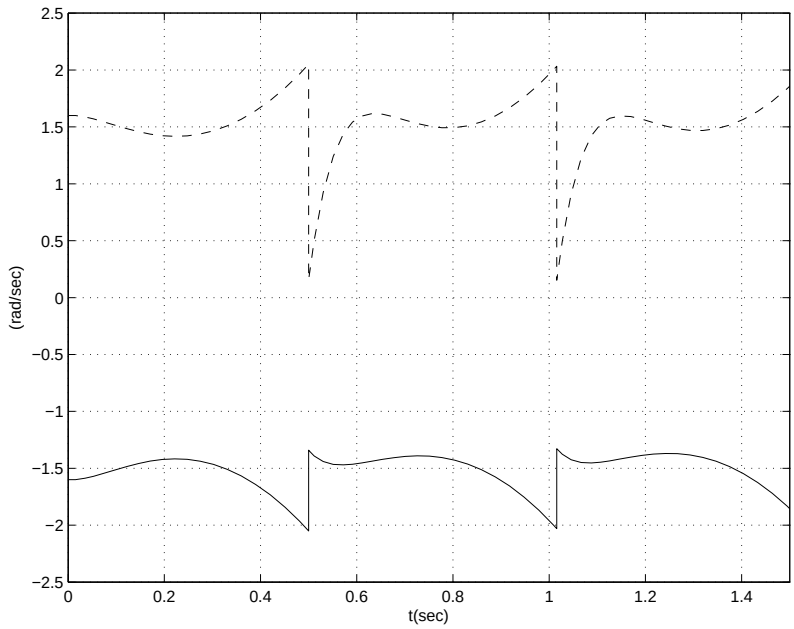

Figure 5.4: The simulation result of the robot showing the joint velocities $\dot{q}_1$ (straight line) and $\dot{q}_2$ (dashed line) versus time.

5.3 Trajectory tracking control with impacts: Bezier approximations

The section 5.2 provided the concept of zero dynamics including the impact condition and the determination of the output functions. In this section, a closed

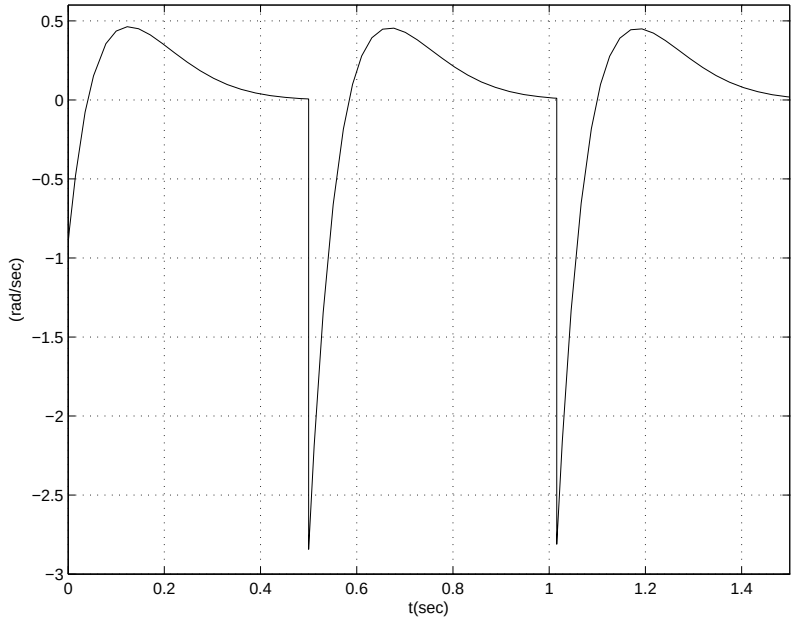

Figure 5.5: The simulation result of the three-link robot for $\dot{q}_3$ versus time.

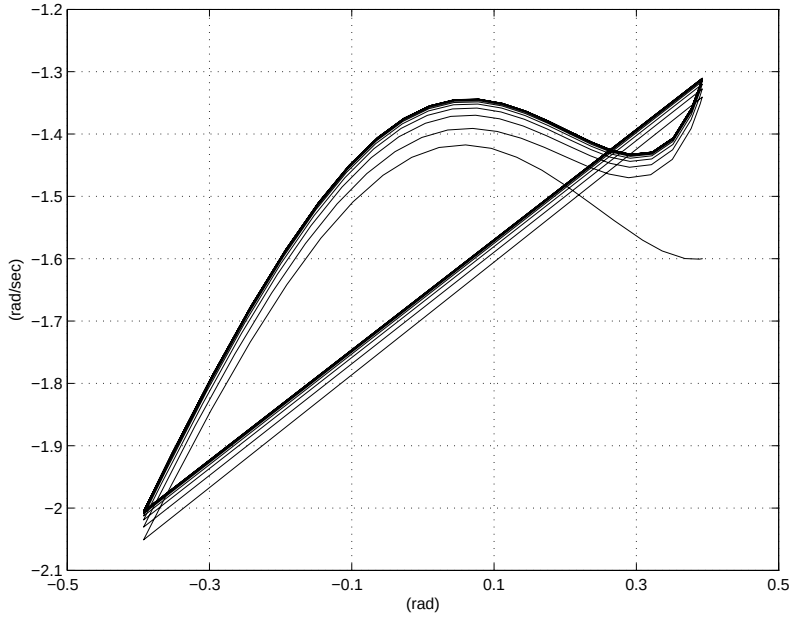

Figure 5.6: Phase portrait of the motion, q_1 versus $\dot{q}_1$. The limit cycle converges to the periodic gait after 10 steps.

from representation of the zero dynamics will be defined and the shaping of the zero dynamics are done by optimization. For achieving this, the output function is parameterized with Bézier polynomials [3]. Rather then tracking an Ad hoc output (5.6) as in the previous case, the outputs are shaped to obtain a stable walking motion. A Bézier polynomial is a smooth curve having control points and

by modifying the control points and the polynomial order, a desired trajectory can be achieved. The output shaping with optimization that is adopted in here, is suggested in [61].

5.3.1 Defining output functions with Bezier polynomials

A class of output functions in a closed-form representation is derived. The output function is defined as

$$y = h(q) = h_0(q) - h_d(\theta) \tag{5.25}$$

where $h_0(q)$ corresponds to the independent controllable variables and $h_d(\theta)$ corresponds to their evolution as a function of $\theta(q)$, with

$$h_0(q) = q_a \tag{5.26}$$

$$\theta(q) = cq. \tag{5.27}$$

Different from the case of trajectory tracking, $\theta(q)$ is used to replace time in parameterizing the motion of the robot. The walking motion is slaved to $\theta(q)$ which is monotonic along its motion. The objective is to determine the $h_d(\theta)$ that is compatible with a periodic motion. Enforcing the virtual constraints to zero $y = h(q) = 0$, results in $q_a = h_d(\theta)$. The virtual constraints are parameterized by Bezier polynomials of order M,

$$b_i(s) = \sum_{k=0}^{M} p(i,k) \frac{M!}{k!(M-k)!} s^k (1-s)^{M-k} \tag{5.28}$$

where $p(i,k)$ are the $M+1$ coefficients.

Bezier polynomial is a smooth curve and its first derivative is derived as

$$\frac{\partial b_i(s)}{\partial s} = \sum_{k=0}^{M-1} (p(i,k+1) - p(i,k)) \frac{M!}{k!(M-k-1)!} s^k (1-s)^{M-k-1}. \tag{5.29}$$

Its values at the initial and final points can be computed as

$$b_i(0) = p(i,0) \qquad \text{and} \qquad b_i(1) = p(i,M), \tag{5.30}$$

$$\frac{\partial b_i(0)}{\partial s} = M(p(i,1) - p(i,0)) \tag{5.31}$$

$$\frac{\partial b_i(1)}{\partial s} = M(p(i,M) - p(i,M-1)). \tag{5.32}$$

where s is the normalized variable $s(q) = \frac{\theta(q)-\theta^+}{\theta^- + \theta^+}$ and θ^- is the value of $\theta(q)$ just before impact, and θ^+ is the value just after impact. Define $h_d(\theta) = [b_1(s)b_2(s)\cdots b_{N-1}(s)]$ where N is the degrees of freedom of the system.

To have a periodic motion, the first and last coefficients of the Bezier polynomials need to satisfy the following equations

$$p(0) = h_d(\theta^+) = q_a^+ \tag{5.33}$$

$$p(M) = h_d(\theta^-) = q_a^-. \tag{5.34}$$

Taking the partial derivatives

$$\begin{aligned}\frac{\partial h_d(\theta)}{\partial \theta} &= \frac{\partial b_i(s)}{\partial s}\frac{\partial s}{\partial \theta} \qquad (5.35)\\ &= \left[\sum_{k=0}^{M-1}(p(i,k+1)-p(i,k))\frac{M!}{k!(M-k-1)!}s^k(1-s)^{M-k-1}\right]\frac{1}{\theta^- - \theta^+}\\ \frac{\partial h_d(\theta^+)}{\partial \theta} &= \frac{M}{\theta^- - \theta^+}(p(1)-p(0)) \qquad (5.36)\\ \frac{\partial h_d(\theta^-)}{\partial \theta} &= \frac{M}{\theta^- - \theta^+}(p(M)-p(M-1)) \qquad (5.37)\\ p(1) &= p(0) + \frac{\theta^- - \theta^+}{M}\frac{\dot{q}_a^+}{\dot{\theta}^+} \qquad (5.38)\\ p(M-1) &= p(M) - \frac{\theta^- - \theta^+}{M}\frac{\dot{q}_a^-}{\dot{\theta}^-} \qquad (5.39)\end{aligned}$$

and the parameters $p_2, \ldots, p_{M-2}$ are the free variables that need to be chosen to obtain a periodic motion.

5.3.2 Parametrization of output functions by optimization

An automated method of searching for periodic gaits is developed to search for the fixed points with an optimization technique. The optimization method is adopted to design trajectories with a minimum cost. It is used to design the desired motion with the selection of the initial conditions, output function parameters and control gains. The goal is to minimize the cost function subject to the following nonlinear inequality and equality constraints:

- The swing foot is above the ground
- θ should be monotonic ($\dot{\theta}$ is not zero)
- An impact occurs

- There exists a fixed point (the solution is periodic)
- There exists a stable fixed point
- The solution is symmetric (with respect to the leg positions)

The cost function is

$$J = \frac{1}{L}\int_0^T \frac{1}{2} u^{*^T} u^* dt \tag{5.40}$$

where T is the period and L is the step length. This optimization problem is solved using constrained nonlinear optimization tool fmincon.

The optimization problem is posed as explained above. In order to execute the optimization cycle, an initial guess for the state is set for the before impact condition, x^-. Then, the impact model is applied to x^- to compute x^+. The output function parameters are set and the robot with the controller is integrated until the impact condition to obtain the new state configuration x^-. Finally, the cost function J is computed. This routine is simulated until a fixed point of the solution is obtained by assigning new initial conditions as the constraints are satisfied with the minimum cost function.

5.3.3 Case study: Three-link planar robot

In this section, simulation results of the three-link planar robot are presented. The equations of motion of the robot are those of a three-link open kinematic chain. Derivations are provided in Section 2.5.2. The derivation of the impact condition is given in Section 2.5.3. The complete model of robot in closed form is expressed in Section 2.5.

The procedure to achieve a stable periodic motion is explained as follows:

1. The initial state x_n^- for the pre-impact condition is set, where n corresponds to the number of steps.
2. Under the impact function post-impact model state is determined.
3. With the definition of the Bézier polynomials, virtual constraints are set and the corresponding feedback controller is designed.

4. The equations of motion are integrated until the impact condition is met resulting in new pre-impact state x_{n+1}^- while satisfying the optimality criterion.

5. The new pre-impact state is compared with the old pre-impact state with the error $x_n^- - x_{n+1}^- = 0$.

6. If the error can not converge to zero, new initial state is attained while satisfying the constraints of the optimization.

Virtual Constraints

The swing phase zero dynamics are applied on the three-link robot to construct a walking motion. The style of walking is discussed in section 5.3.2. The output is defined as

$$y = q_a - h_d(\theta), \tag{5.41}$$

where $\theta = q_1$. The q_a defines the actuated coordinates, q_2 and q_3. The outputs are parameterized by Bezier polynomials of order 3.

Controller

A control law for exactly tracking the output functions is investigated. The nonlinear model can be locally asymptotically stabilized with the definition of output feedback as an inner feedback loop control. The effectiveness of the controller relies on eliminating errors due to impacts during subsequent steps. High-gain approach ensures convergence and is robust to noise and uncertainty. Thus, the high-gain controller is used as proposed in [29]. The feedback is defined as

$$u(x) = -(L_g L_f h(x))^{-1}(\nu - L_f^2 h(x)), \tag{5.42}$$

with

$$\nu = \frac{K_p}{\epsilon^2} y + \frac{K_d}{\epsilon} \dot{y}. \tag{5.43}$$

Simulation results

The three-link model is simulated and the nonlinear equations of motion are integrated with a $4th - 5th$ order automatic step-sizing routine. An integration tolerance of 10^{-5} is used.

The robot's initial conditions are

$$q_1 = -0.3927 \tag{5.44}$$

$$q_2 = 0.3927 \tag{5.45}$$

$$q_3 = -0.5236 \tag{5.46}$$

$$\dot{q}_1 = -1.5044 \tag{5.47}$$

$$\dot{q}_2 = 1.1069 \tag{5.48}$$

$$\dot{q}_3 = -0.0618. \tag{5.49}$$

The equations are integrated until the switching condition

$$S = \{(q, \dot{q}) \in X \mid h = 0, L > 0\} \tag{5.50}$$

is met where

$$h = l_1 cos(q_1) - l_2 cos(q_2) \quad \text{and} \quad L = -l_1 sin(q_1) + l_2 sin(q_2). \tag{5.51}$$

The feedback is assigned as

$$\nu = \frac{K_p}{\epsilon^2} y + \frac{K_d}{\epsilon} \dot{y}. \tag{5.52}$$

with $\epsilon = 0.1$, $K_p = -149.9846$ and $K_d = 0$. The fixed point for the periodic and symmetric walking cycle is obtained as

$$x^* = [q^*, \dot{q}^*] \tag{5.53}$$

$$= [\ -0.3927 \quad 0.3927 \quad -0.5236 \quad -1.5044 \quad 1.1069 \quad -0.0618\ ]. \tag{5.54}$$

The computed eigenvalues of the linearized Poincaré map are

$$\sigma = [\ 0 \quad 0.6916 + 0.4393i \quad 0.6916 - 0.4393i \quad 0.8657 \quad 1.0000 \quad 0.9907\ ]. \tag{5.55}$$

One of the eigenvalues is exactly equal to one and others have magnitude strictly less than one. The orbit corresponding to the fixed point is asymptotically stable.

The stick figure of the robot shown in Figure 5.7 illustrates the motion of the system for one step. The model's angular coordinates for the leg trajectories over 3 steps are shown in Figure 5.8. The straight lines in the configuration coordinates correspond to the impact condition. Figure 5.9 presents the configuration trajectory of the torso.

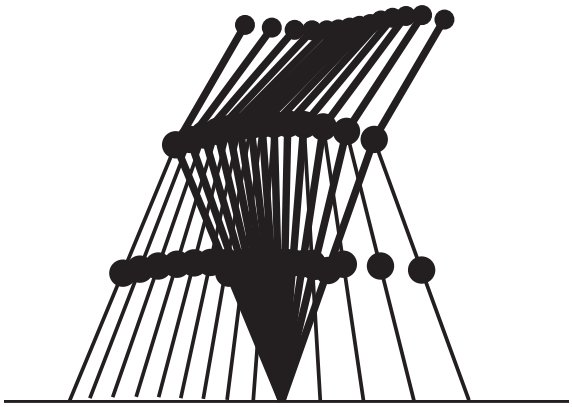

Figure 5.7: Stick figure of the robot.

The feedback control method is applied on the three-link planar robot which resulted in a locally asymptotically stable walking motion. Periodic motions around a specific equilibrium point is formulated with the addition of impacts to ensure that walking is achieved. Existence of these periodic motions and their stability are provided with Poincaré mapping. The choice of the control method is crucial in the design process. The stability of walking motion heavily relies on the effectiveness of the controller to compensate for the effects of impact.

Although this model does not have a very human-like architecture, it highlights the possibility of dynamic walking. This model can be extended to include knees and feet to obtain a general walking model. Achieving dynamic walking without falling under tolerable disturbances can be next considered to resemble human like motion. The tracking errors in control can lead to stable trajectories whereas they are different than the intended motion. The parameter space can be partitioned to overcome this difficulty where the control action chooses the closest stable trajectory.

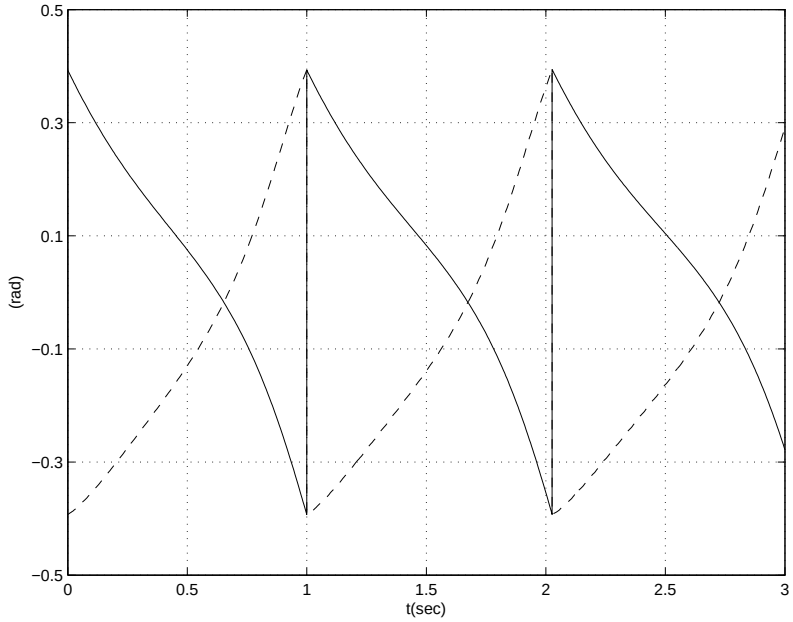

Figure 5.8: The simulation result of the robot showing the leg angles q_1 (straight line) and q_2 (dashed line) for 3 steps. The straight lines corresponds to the impacts.

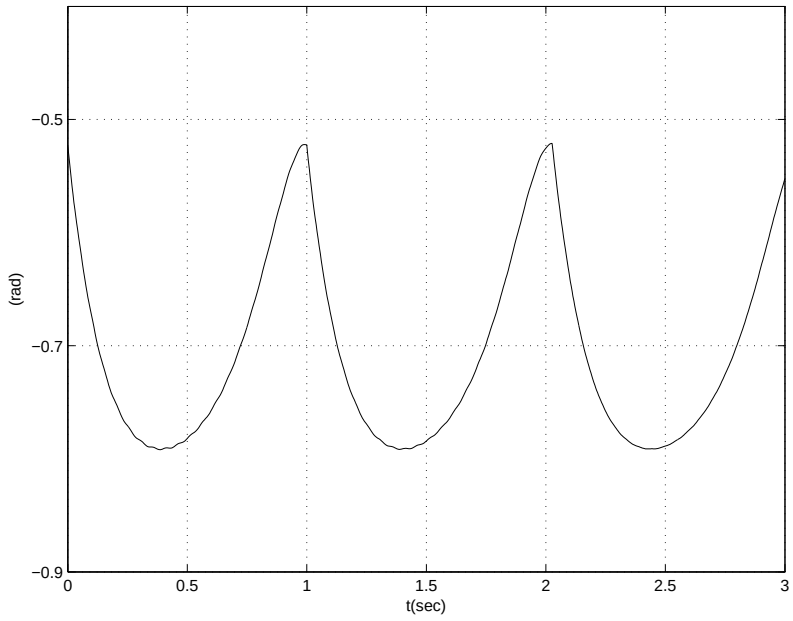

Figure 5.9: The simulation result of the robot showing the torso angle q_3.

Chapter 6

Conclusion and Future Work

6.1 Conclusion

Stability is one of the major concepts in biped locomotion since an unstable biped has the risk of falling during its motion. The biped's high center of mass position needs to be maintained well enough over its relatively small support area. Flat-footed robots can achieve this by keeping their center of mass within their support foot area, however, in the case of single point contact with the ground, the balance control of biped becomes complex. Static stability is no longer desirable as the center of mass leaves the contact point during its motion. In order to address this dynamic stability problem, a class of underactuated mechanical systems are studied that are chosen simple enough to cast the dynamic stability problem in robot balancing and walking.

A two-link robot and a three-link robot are controlled to track stable periodic orbits for achieving the dynamic balancing and walking tasks. The two-link robot with only one actuation at the hip and the links representing the lower and upper bodies of a biped, is adopted to simulate the balancing control with torso rotation. In the case of small disturbances, balancing the two-link robot with hip actuation is presented. Walking is a type of balancing task with support changes and impacts. The robot is assumed to have three links with two legs, a torso and point feet without any actuation at the contact between the feet and the ground. The planar biped is studied for casting the essential points in walking with the problem of underactuation, impact condition and dynamic stability.

In this thesis, stable periodic orbits are tracked by developing feedback controllers for the treated models. In particular, periodic trajectories of these sys-

tems are shaped by designing output functions to encode the robot's posture using Bézier polynomial approximations and parameter optimization techniques. The output functions that are named as virtual constraints are imposed on the system by feedback. Feedback controllers with partial feedback linearization and high-gain approaches are derived to satisfy the virtual constraints. Then, stability of the closed-loop systems are analyzed. Finally, the control method implementations are presented with simulations.

The summary of this thesis is as follows.

In Chapter 1, an introduction over the underactuated mechanical systems and biped locomotion are provided.

In Chapter 2, the dynamics of the two-link and three-link planar robots are defined using Kane's method.

The control of the underactuated mechanical systems with partial feedback linearization are introduced in Chapters 3-5. These examples are provided with detailed control design and simulation results. In Chapter 3, the swing-up and balancing control problem of the two-link planar robot is studied with noncollocated feedback linearization method. The robot is stabilized around its inverted condition.

In Chapter 4, with the introduction of an output function, a trajectory is addressed for the two-link planar robot. The behavior of the system is realized according to the enforced output and zeroing the output results in zero dynamics. The stability of the system is analyzed by studying the zero dynamics stability.

In Chapter 5, partial feedback linearization method is applied on the three-link planar robot to achieve walking motion. This motion is encoded into the system by defining a set of outputs and zeroing these outputs enforces the system to attain the gait coordination. The defined trajectory is parameterized by the system states rather than by time such that a time-independent motion is designed. Additional to the Ad hoc output design, a new set of outputs are defined that are parameterized with Bézier approximations. The output function is optimized by using the parameter optimization techniques. Stability of periodic motions of the switching model is analyzed with the Poincaré mapping.

6.2 Future Work

The principles discussed in this thesis are applicable to a large class of biped robot control problems. In this section, the potential future research topics as extensions to this work are provided.

A new stable and periodic walking structure has been investigated and yet to be developed. One step cycle is divided into phases where the robot can switch between them in the case of balance loss. With the modification in gait shaping stage, one step will be divided into phases to realize the switching property within gaits. The robot can keep its balance under disturbances by switching to the closest stable trajectory or converge to a closest point in its equilibrium manifold. This idea is still under investigation.

The biped robot that is treated in this thesis does not have flat feet and respectively there is no actuation at the ankles. Additional to dynamic walking, biped robots may also need to demonstrate static stability in necessary conditions and structured environments. Considering that, with the addition of feet, the robustness of the biped will be improved.

The control problem of biped walking is studied for planar bipeds. For real life robots, the results may be generalized to three-dimensional biped models.

Appendix A

Derivation of the Equations of Motion

The equations of motion for the two-link planar robot are derived by the Kane's method [30]. The three-link planar robot's equations can be derived with the same method as explained below.

A.1 Definitions

In order to formulate the equations of motion, the symbols for bodies, points, constants, variables, basis vectors and generalized coordinates are defined. The Figure 2.2 shows the two-link robot defining the symbols. The robot consists of two rigid links A and B with masses M_1, M_2. The point O is the center of the fixed horizontal axis where the body A rotates about and the body B rotates about the horizontal axis fixed in A. The point A_o, representing the mass center of A, lies a distance l_{c1} from O. The mass center of B, B_o, is located a distance l_{c2} from the point AB, the joint connection of A and B. The end point of the body B is E. The length of bodies are represented by l_1 and l_2. The variable is the torque $T_{A/B}$, applied to link B by an actuator attached to A. The unit vectors are N_i $(i = 1, 2, 3)$, fixed in an inertial reference frame N. Respectively, A_i and B_i are fixed in A and B.

A.2 Generalized coordinates and speeds

The generalized coordinates describe the configuration of the system as the generalized speeds describe the motion of the system. Generalized coordinates for the system are chosen in joint space as q_1 and q_2. q_1 is the angle between N_2 and A_1 and q_2 is the angle between A_1 and B_1. The generalized speeds are introduced as the first time derivative of the corresponding generalized coordinate. The generalized coordinate derivatives represented with the generalized speeds are called the kinematical differential equations are defined as

$$\dot{q}_1 = u_1 \tag{A.1}$$

$$\dot{q}_2 = u_2. \tag{A.2}$$

A.3 Velocities

The angular velocities of bodies A and B and the translational velocities of the points A_o, B_o, AB, E are derived in reference frame N. The angular velocities are

$$\omega^A = u_1 A_3 \tag{A.3}$$

$$\omega^B = u_1 A_3 + u_2 B_3. \tag{A.4}$$

The translational velocities are derived by relating the velocities of two points fixed on a single rigid body. The velocities of points A_o, B_o, AB, E are

$$v^{A_o} = l_{c1} u_1 A_2 \tag{A.5}$$

$$v^{B_o} = l_1 u_1 A_2 + l_{c2}(u_1 + u_2) B_2 \tag{A.6}$$

$$v^{AB} = l_1 u_1 A_2 \tag{A.7}$$

$$v^{E} = l_1 u_1 A_2 + l_2(u_1 + u_2) B_2 \tag{A.8}$$

$$\tag{A.9}$$

A.4 Partial Velocities

Partial velocities are developed from the angular velocities of the nonmassless bodies and the bodies that contribute to the equations of motions which are acted

by torques. Additionally it is derived from the translational velocities of of the nonmassless particles and the particles that contribute to the equations of motions where forces are applied. These partial velocities are the coefficients of the generalized speeds. .

x	r=1	r=2
ω_r^A	A_3	0
ω_r^B	0	B_3
$v_r^{A_o}$	$l_{c1}A_2$	0
$v_r^{B_o}$	$l_1A_2 + l_{c2}B_2$	$l_{c2}B_2$
v_r^{AB}	l_1A_2	0
v_r^E	$l_1A_2 + l_2B_2$	l_2B_2

Table A.1: Partial velocities

A.5 Accelerations

The accelerations are derived by direct differentiation or applying the kinematic formula. The angular accelerations are derived by differentiating the angular velocities

$$\alpha^A = \dot{u}_1 A_3 \tag{A.10}$$

$$\alpha^B = (\dot{u}_1 + \dot{u}_2) B_3. \tag{A.11}$$

The translational accelerations of the particles and body mass centers are

$$a_r^{A_o} = -l_{c1}u_1^2 A_1 + l_{c1}\dot{u}_1 A_2 \tag{A.12}$$

$$a_r^{B_o} = -l_1 u_1^2 A_1 + l_1 \dot{u}_1 A_2 - l_{c2}(u_1 + u_2)^2 B_1 + l_{c2}(\dot{u}_1 + \dot{u}_2) B_2 \tag{A.13}$$

$$a_r^{AB} = -l_1 u_1^2 A_1 + l_1 \dot{u}_1 A_2 \tag{A.14}$$

$$a_r^E = -l_1 u_1^2 A_1 + l_1 \dot{u}_1 A_2 - l_2(u_1 + u_2)^2 B_1 + l_2(\dot{u}_1 + \dot{u}_2) B_2. \tag{A.15}$$

A.6 Generalized Inertia Forces

The generalized inertia forces F_r^* in a reference frame N is defined as

$$F_r^* = -\sum_{i=1}^{n} v_r^{P_i} \cdot m_i a^{P_i} \qquad (r = 1, \ldots, n). \tag{A.16}$$

$v_r^{P_i}$ is the rth partial velocity of particle P_i. The generalized inertia forces for the system are

$$F_1^* = -l_1 l_{c2} M_2 \sin(q_2)(u_1^2 - (u_1 + u_2)^2) - (l_{c2} M_2 (l_{c2} + l_1 \cos(q_2)))\dot{u}_2 \quad \text{(A.17)}$$
$$-(M_1 l_{c1}^2 + M_2 (l_1^2 + l_{c2}^2 + 2 l_1 l_{c2} \cos(q_2)))\dot{u}_1$$

$$F_2^* = -l_1 l_{c2} M_2 \sin(q_2) u_1^2 - (M_2 l_{c2}^2)\dot{u}_2 - (l_{c2} M_2 (l_{c2} + l_1 \cos(q_2)))\dot{u}_1 \quad \text{(A.18)}$$

A.7 Generalized Active Forces

The non-working forces or torques are orthogonal to the tangent space of the configuration or motion manifold and thus they do no work on the system. The gravitational force and the torque are active forces acting on the system. Because of that reason the generalized active forces are introduced. The generalized active forces are determined by multiplying the contributing forces and torques with partial velocities of the points and bodies that are applied to and are given as

$$F_1 = -g(l_{c1} M_1 \cos(q_1) + M_2 (l_1 \cos(q_1) + l_{c2} + \cos(q_1 + q_2))) \quad \text{(A.19)}$$

$$F_2 = T_{A/B} - g l_{c2} M_2 \cos(q_1 + q_2). \quad \text{(A.20)}$$

A.8 Equations of Motion

The dynamical differential equations of the system can be determined by

$$F_r + F_r^* = 0 \qquad (r = 1, 2). \quad \text{(A.21)}$$

Appendix B

Conservation of Angular Momentum

In this appendix, the conservation of angular momentum for the three-link planar robot at the impact is explained.

The kinematic chain is shown in Figure B.1. When the swing foot touches the ground, the impact occurs. Based on the assumptions clarified previously

1. Ground contact generates jumps in the velocity vector, while position remains constant,
2. no rebound and no slipping of the swing leg
3. The double support phase is instantaneous

the angular momentum is conserved for the entire system about the swing foot contact point, for the new swing leg about the hip joint and for the torso about the hip joint. These conservation equations can be written as

$$H_E^- = H_E^+ \tag{B.1}$$

$$H_H^{-st} = H_H^{+sw} \tag{B.2}$$

$$H_H^{-torso} = H_H^{+torso}. \tag{B.3}$$

According to the notation, the + superscript means post-impact and − superscript means pre-impact.

In order to formulate the equations of motion, the symbols for bodies, points, constants, variables, basis vectors and generalized coordinates are denoted as explained in Appendix A. The linear velocities are determined. With these notations, the conservation of angular momentum equations are written as follows,

$$M_1 v^{-A_o} \times \vec{P}_{E/A_o} + M_2 v^{-B_o} \times \vec{P}_{E/B_o} + M_3 v^{-C_o} \times \vec{P}_{E/C_o} + M_h v^{-H} \times \vec{P}_{E/H} \quad \text{(B.4)}$$
$$= M_1 v^{+A_o} \times \vec{P}_{E/A_o} + M_2 v^{+B_o} \times \vec{P}_{E/B_o} + M_3 v^{+C_o} \times \vec{P}_{E/C_o} + M_h v^{+H} \times \vec{P}_{E/H}$$

$$M_2 v^{-B_o} \times \vec{P}_{H/B_o} = M_2 v^{+B_o} \times \vec{P}_{H/B_o} \quad \text{(B.5)}$$

$$M_3 v^{-C_o} \times \vec{P}_{H/C_o} = M_3 v^{+C_o} \times \vec{P}_{H/C_o}. \quad \text{(B.6)}$$

The center of mass positions are named by denoting the endpoints for example $\vec{P}_{E/A_o}$ corresponds to the distance connecting the point E to the point mass A_o. The center of mass velocities are denoted according to their corresponding bodies and points. The superscripts $+$ and $-$ mean pre- and post- collision velocities.

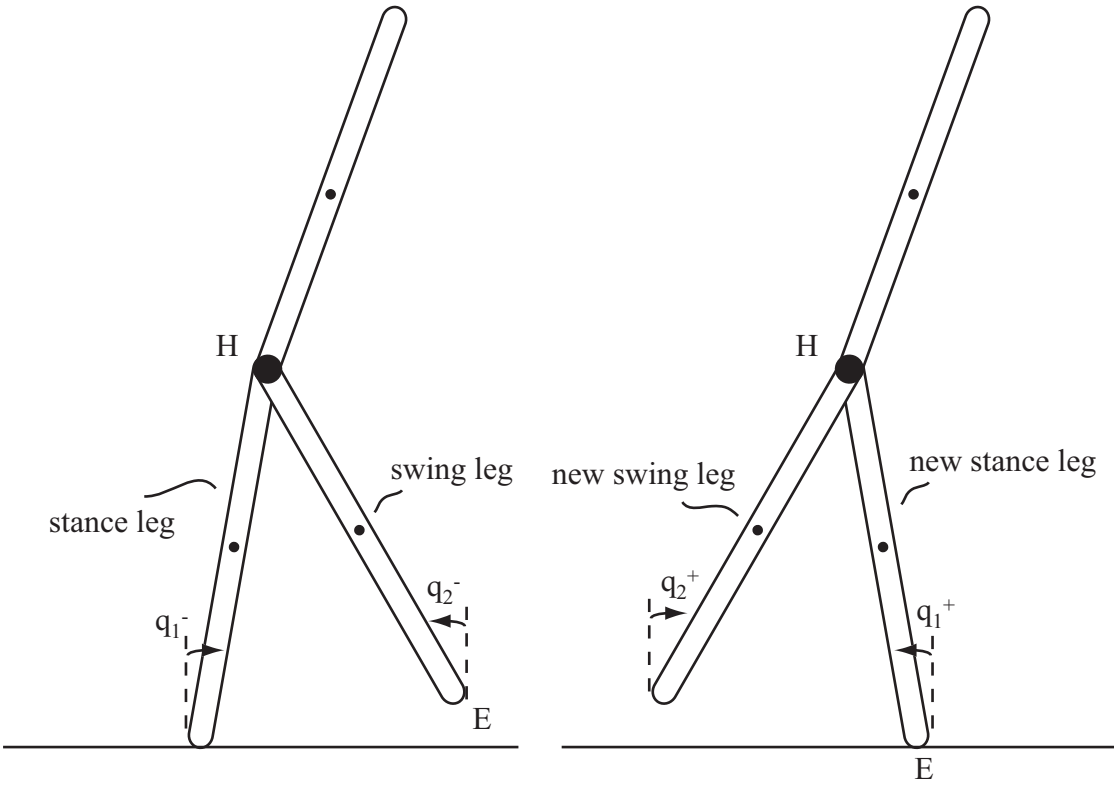

Figure B.1: Conservation of the angular momentum: pre- and post- collision configurations. The angular momentum is conserved around the contact point E for the entire system and around hip joint H for the new swing leg and torso.

The matrices Q^+ and Q^- of the conservation equations have entries

$$Q^-(1,1) = I_1 + l_1 l_2 M_h cos(q_1 - q_2) + l_1 M_2 (l_2 - l_{c2}) cos(q_1 - q_2) +$$
$$l_1 M_3 (l_2 cos(q_1 - q_2) + l_{c3} cos(q_1 - q_3)) - l_{c1} M_1 (l_1 - l_{c1} - l_2 cos(q_1 - q_2))$$

$$Q^-(1,2) = I_2 - l_{c2} M_2 (l_2 - l_{c2})$$

$$Q^-(1,3) = I_3 + l_{c3} M_3 (l_{c3} + l_2 cos(q_2 - q_3))$$

$$Q^-(2,1) = I_1 - l_{c1} M_1 (l_1 - l_{c1})$$

$$Q^-(2,1) = 0$$

$$Q^-(2,3) = 0$$

$$Q^-(3,1) = l_1 l_{c3} M_3 cos(q_1 - q_3)$$

$$Q^-(3,2) = 0$$

$$Q^-(3,3) = I_3 + M_3 l_{c3}^2$$

$$Q^+(1,1) = I_1 + M_1 l_{c1}^2 + M_h l_1^2 + l_1 M_3 (l_1 + l_{c3} cos(q_1 - q_3)) + l_1 M_2 (l_1 - l_{c2} cos(q_1 - q_2))$$

$$Q^+(2,1) = I_2 + l_{c2} M_2 (l_{c2} - l_1 cos(q_1 - q_2))$$

$$Q^+(3,1) = I_3 + l_{c3} M_3 (l_{c3} + l_1 cos(q_1 - q_3))$$

$$Q^+(2,1) = -l_1 l_{c2} M_2 cos(q_1 - q_2)$$

$$Q^+(2,2) = I_2 + M_2 l_{c2}^2$$

$$Q^+(2,3) = 0$$

$$Q^+(3,1) = l_1 l_{c3} M_3 cos(q_1 - q_3)$$

$$Q^+(3,2) = 0$$

$$Q^+(3,3) = I_3 + M_3 l_{c3}^2$$

Bibliography

[1] K.J. Astrom and K. Furuta, *Swining up a pendulum by energy control*, IFAC (San Francisco), 1996.

[2] M.D. Berkemeier and R.S. Fearing, *Sliding and hopping gaits for the underactuated acrobot*, IEEE Transactions on Robotics and Automation **14** (1998), no. 4, 629–634.

[3] P. Bézier, *Numerical control: Mathematics and applications*, John Wiley & Sons, New York, 1972.

[4] S.P. Bhat and D.S. Bernstein, *Continuous finite-time stabilization of the translational and rotational double integrators*, IEEE Transactions on Automatic Control **43** (1998), no. 5, 678–682.

[5] S. Bortoff and M.W. Spong, *Pseudolinearization of the acrobot using spline functions*, Proc. IEEE Conf. on Decision and Control (1992), 593–598.

[6] R.W. Brockett, *Differential geometric control theorey*, Birkhauser, 1983.

[7] C. Chevallereau, *Time-scaling control for an underactuated biped robot*, IEEE Transactions on Robotics and Automation **19** (2003), no. 2, 362–368.

[8] C. Chevallereau, G. Abba, Y. Aoustin, F. Plestan, E.R. Westervelt, C. Canduas de Wit, and J.W. Grizzle, *Rabbit: A testbed for advanced control theory*, IEEE Control Systems Magazine **23** (2003), no. 5, 57–79.

[9] C. Chevallereau, A. Formalsky, and D. Djoudi, *Tracking a joint path for the walk of an underactuated biped*, Robotica **22** (2004), no. 1, 15–28.

[10] C.C. Chung and J. Hauser, *Nonlinear control of a swinging pendulum*, Automatica **40** (1995), 851–862.

[11] M.J. Coleman, M. Garcia, K. Mombaur, and A. Ruina, *Prediction of stable walking for a toy that cannot stand*, Physical Review E **64** (2001), no. 2, 022901–1 – 022901–3.

[12] S.H. Collins, M. Wisse, and A. Ruina, *A two legged kneed passive dynamic walking robot*, International Journal of Robotics Research **20** (2001), no. 7, 607–615.

[13] K. Erbatur, U. Seven, E. Taskıran, O. Koca, M. Yılmaz, M. Unel, G. Kızıltas, A. Sabanovic, and A. Onat, *Suralp: A new full-body humanoid robot platform*, Intelligent Robots and Systems, 2009. IROS 2009. IEEE/RSJ International Conference on (2009), 4949–4954.

[14] B. Espiau, *Bip: a joint project for the development of an anthropomorphic biped robot*, Proc. of the International Conference on Advanced Robotics (1997), 267–272.

[15] J. Furusho and M. Masubuchi, *Control of a dynamical biped locomotion system for steady walking*, Journal of Dynamic Systems, Measurement, and Control **108** (1986), 111–118.

[16] M. Garcia, A. Chatterjee, and A. Ruina, *Efficiency, speed, and scaling of two-dimensional passive-dynamic walking*, Dynamics and Stability of Systems **15** (2000), no. 2, 75–99.

[17] M. Garcia, A. Chatterjee, A. Ruina, and M.D. Coleman, *The simplest walking model: Stability, complexity, and scaling*, ASME J. Bzomech. Eng. **120** (1998), no. 2, 281–288.

[18] M. Gienger, K. Löffler, and F. Pfeiffer, *A biped robot that jogs*, Proc. of the IEEE International Conference on Robotics and Automation (2000), 3334–3339.

[19] A. Goswami, B. Espiau, and A. Keramane, *Limit cycles and their stability in a passive bipedal gait*, Proc. of the IEEE International Conference on Robotics and Automation (1996), 246–251.

[20] J.W. Grizzle, G. Abba, and F. Plestan, *Proving asymptotic stability of a walking cycle for a five dof biped robot model*, 2nd Int. Conf. on Climbing and Walking Robots, CLAWAR-99, Portsmouth, U.K. (1999), 69–81.

[21] ———, *Asymptotically stable walking for biped robots: Analysis via systems with impulse effects*, IEEE Transactions on Automatic Control **46** (2001), 51–64.

[22] Y.L. Gu, *A direct adaptive control scheme for underactuated dynamic systems*, Proc. IEEE Conf. on Decision and Control (1993), 1625–1627.

[23] J. Hale, *Ordinary differential equations*, Krieger, Malabar, FL, USA, 1980.

[24] J. Hauser and R.M. Murray, *Nonlinear controllers for non-integrable systems: the acrobot example*, Proceedings of American Control Conference (1990), 669–670.

[25] K. Hirai, M. Hirose, Y. Haikawa, and T. Takenake, *The development of honda humanoid robot*, In Proc. of the IEEE International Conference on Robotics and Automation, Leuven, Belgium (1998), 1321–1326.

[26] Y. Hürmüzlü, *Dynamics of bipedal gaitpart 1: objective functions and the contact event of a planar five-link biped*, Journal of Applied Mechanics **60** (1993), 331–336.

[27] ———, *Dynamics of bipedal gaitpart 2: Stability analysis of a planar five link biped*, Journal of Applied Mechanics **60** (1993), 337–343.

[28] Y. Hürmüzlü and D.B. Marghitu, *Rigid body collisions of planar kinematic chains with multiple contact points*, International Journal of Robotics Research **13** (1994), no. 1, 82–92.

[29] A. Isidori, *Nonlinear control systems: An introduction*, third ed., Springer-Verlag, Berlin, 1995.

[30] T.R. Kane and D.A. Levinson, *Dynamics: Theory and applications*, McGraw-Hill Book Co., New York, 1985.

[31] I. Kato and H. Tsuiki, *The hydraulically powered biped walking machine with a high carrying capacity*, Proc. of the fourth International Symposium on External Control of Human Extremities (1972), 410–421.

[32] H.K. Khalil, *Nonlinear systems*, Prentice Hall, 2002.

[33] D.D. Koditschek and M. Buhler, *Analysis of a simplified hopping robot*, International Journal of Robotics Research **10** (1991), no. 6, 587–605.

[34] D.E. Koditschek, *Dynamically dexterous robots*, Robot Control:Dynamics, Motion Planning and Analysis (1993), 487–490.

[35] F. Mazenc and L. Praly, *Adding integrations, saturated controls, and stabilization for feedforward systems*, IEEE Trans. on Automatic Control **40** (1996), 1559–1578.

[36] T.G. McGee and M.W. Spong, *Trajectory planning and control of a novel walking biped*, IEEE International Conference on Control Applications, Mexico City, Mexico (2001), 1099–1104.

[37] T. McGeer, *Passive dynamic walking*, International Journal of Robotics Research **9** (1990), no. 2, 62–82.

[38] K. Mitobe, N. Mori, K. Aida, and Y. Nasu, *Nonlinear feedback control of a biped walking robot*, IEEE International Conference on Robotics and Automation, Nagoya, Japan (1995), 2865–2870.

[39] H. Nijmeijer and A.J. van der Schaft, *Nonlinear dynamical control systems*, Springer-Verlag, Berlin, 1989.

[40] K. Ono, R. Takahashi, and T. Shimada, *Self-excited walking of a biped mechanism*, International Journal of Robotics Research **20** (2001), no. 12, 953–966.

[41] J.H. Park and K.D. Kim, *Biped robot walking using gravity-compensated inverted pendulum mode and computed torque control*, Proc. of the IEEE International Conference on Robotics and Automation, Leuven, Belgium (1998), 3528–3533.

[42] J. Pratt, C. Chee-Meng, A. Torres, P. Dilworth, and G. Pratt, *Virtual model control: an intuitive approach for bipedal locomotion*, International Journal of Robotics Research **20** (2001), 129–143.

[43] J. Pratt and G. Pratt, *Exploiting natural dynamics in the control of a 3d bipedal walking simulation*, In Pmc. International Conference on Climbing and Walking Robots, CLAWAR, Portsmouth, UK (1999).

[44] J.E. Pratt and G.A. Pratt, *Intuitive control of a planar bipedal walking robot*, Proc. of the IEEE International Conference on Robotics and Automation, Leuven, Belgium (1998), 2014–2021.

[45] M.H. Raibert, *Legged robots that balance*, MIT Press, Mass., 1986.

[46] M.H. Raibert, S. Tzafestas, and C. Tzafestas, *Comparative simulation study of three control techniques applied to a biped robot*, Proc. of the IEEE International Conference on Systems, Man and Cybernetics Systems Engineering in the Service of Humans (1993), 494–502.

[47] M. Reyhanoglu, A. van der Schaft, and N.H. McClamroch, *Dynamics and control of second-order nonholonomic systems*, Proc. 35th IEEE Conf. Decision Contr. (1996).

[48] F. Saito, T. Fukuda, and F. Arai, *Swing and locomotion control for a two-link brachiation robot*, IEEE Contr. Syst. Mag. **14** (Feb. 1994), 5–12.

[49] A. Sano and J. Furusho, *Realization of natural dynamic walking using the angular momentum information*, Proc. of the IEEE International Conference on Robotics and Automation (1990), 1476–1481.

[50] C.L. Shih and W.A. Gruver, *Control of a biped robot in the double-support phase*, IEEE Transactions on Systems, Man, and Cybernetics **22** (1992), no. 4, 729–735.

[51] M.W. Spong, *The swing up control problem for the acrobot*, IEEE Control Systems Magazine **15** (1995), no. 1, 49–55.

[52] ———, *Energy based control of a class of underactuated mechanical systems*, 1996 IFAC World Congress (1996).

[53] ———, *Applications of switching control in robot locomotion*, Proc. Workshop on Intelligent Control in Robotics and Automation, IFAC World Congress, Beijing, China (1999).

[54] ———, *Passivity-based control of the compass gait biped*, IFAC World Congress, Beijing, China (1999).

[55] M.W. Spong and D.J. Block, *The pendubot: a mechatronic system for control, research and education*, Procedeings of the 34th IEEE Conference on Decision and Control (New Orleans), Dec. 1995, pp. 555–556.

[56] M.W. Spong and F. Bullo, *Controlled symmetries and passive walking*, In IFAC World Congress, Barcelona, Spain, (2002).

[57] M.W. Spong and L. Praly, *Control of underactuated mechanical systems using switching and saturation*, Proc. of the Block Island Workshop on Control Using Logic Based switching (1996).

[58] C.Y. Su and Y. Stepanenko, *Sliding mode control of nonholonomic systems: Underactuated manipulator case*, Proc. IFAC Nonlinear Control Systems Design (1995), 609–613.

[59] B. Thuilot, A. Goswami, and B. Espiau, *Bifurcation and chaos in a simple passive bipedal gait*, Proc. of the IEEE International Conference on Robotics and Automation, Albuquerque, N.M. (1997), 792–798.

[60] M. Vukobratovic, *How to control the artificial anthropomorphic systems.*, IEEE Pans. System, Man and Cybernetics SMC-3 (1973), 497–507.

[61] E.R. Westervelt, J.W. Grizzle, and D. Koditschek, *Hybrid zero dynamics of planar biped walkers*, IEEE Transactions on Automatic Control **48** (2003), no. 1, 42–56.

[62] M. Wisse, A.L. Schwab, and F.C.T. van der Helm, *Passive dynamic walking model with upper body*, Robotica **22** (2004), no. 6, 681–688.